Lithos 206–207 (2014) 384–399

Contents lists available at ScienceDirect

Lithos

journal homepage: www.elsevier.com/locate/lithos

Eocene supra-subduction zone mafic magmatism in the Sibumasu Block of SW Yunnan: Implications for Neotethyan subduction and India–Asia collision

Yuejun Wang [a,b,*], Limin Zhang [a,b], Peter A. Cawood [c,d], Liyan Ma [e], Weiming Fan [f], Aimei Zhang [g], Yuzhi Zhang [a,b], Xianwu Bi [h]

[a] Department of Earth Sciences, Sun Yat-Sen University, Guangzhou 510275, China
[b] Guangdong Provincial Key Laboratory of Mineral Resources and Geological Processes, Guangzhou 510275, China
[c] Department of Earth Sciences, University of St. Andrews, St. Andrews, UK
[d] School of Earth and Environment, University of Western Australia, Crawley, 35 Stirling Highway, Australia
[e] College of Earth Sciences, Guilin University of Technology, Guilin 541004, China
[f] Key Laboratory of Continental Collision and Plateau Uplift, Institute of Tibetan Plateau Research, Chinese Academy of Sciences, Beijing 100101, China
[g] Third Institute of Oceanography, State Oceanic Administration, Xiamen 361005, China
[h] State Key Laboratory of Ore Deport Geochemistry, Institute of Geochemistry, Chinese Academy of Sciences, Guiyang 550002, China

ARTICLE INFO

Article history:
Received 11 April 2014
Accepted 9 August 2014
Available online 21 August 2014

Keywords:
Early Eocene mafic rocks
Mantle source
Geochronological and geochemical constrains
Gangdese belt
Neotethyan suprasubduction
NW Yunnan

ABSTRACT

Geochemical and isotopic data for metabasic rocks in NW Yunnan constrain the nature of the mantle source beneath the East Himalayan Syntaxis during the Neotethyan subduction and the timing of initial collision between India and Asia. Our results indicate that these mafic rocks crystallized at 50–55 Ma and were metamorphosed at ~39 Ma, contemporaneous with magmatic flare-ups and high-grade metamorphism in South Tibet. The mafic rocks in NW Yunnan are divisible into three groups. Group 1, from Nabang, shows geochemical affinity to a MORB-like source modified by the recycled component with $\varepsilon_{Nd}(t)$ of +5.1 to +9.5 and $\varepsilon_{Hf}(t)$ of +5.1 to +11.6, and resembles back-arc basin basalt. Group 2 is mainly from Jinzhouzhai and Tongbiguan to the east of Group 1, and is marked by high Al_2O_3, enrichment in LILEs and depletion in HFSEs, along with negative $\varepsilon_{Nd}(t)$ (−1.1 to −5.6) and $\varepsilon_{Hf}(t)$ (−4.6 to −0.9) values. Group 2 is interpreted to have originated from the lithospheric mantle modified by input from a slab-derived component in a continental arc setting. Group 3, from Nanjingli, is located a considerable distance east from Group 1, and exhibits negative $\varepsilon_{Nd}(t)$ (−6.7 to −7.6) and $\varepsilon_{Hf}(t)$ (−7.1 to −2.2), and is inferred to be derived from the Tengchong lithospheric mantle but with limited involvement of a slab-derived component. Overall Nd–Hf isotopic compositions show a sharp decrease from Group 1 to Group 2 and then a more subdued decrease to Group 3, with the three groups corresponding to an overall spatial distribution from west to east. Our results suggest that early Eocene magmatism in NW Yunnan represents the eastward continuation of the Gangdese magmatic belt and that the Neotethyan subduction continued until ~50 Ma followed by the India–Asia collision. It is proposed that at least two eastward-dipping subduction zones are involved in the Neotethyan suprasubduction system prior to 55 Ma. The sudden decrease in convergence rate in the early Eocene (55–50 Ma), together with the inferred positive buoyancy of the Tengchong lithosphere, stimulated rollback of down-going slab and induced melting of heterogeneous mantle sources to result in a flare-up in magmatic activity.

1. Introduction

A suite of geological processes involving Tethyan subduction, block amalgamation, and indentation and accretion of India against and beneath Asia resulted in the formation of the Tibetan plateau (e.g., Dewey et al., 1988; Ding et al., 2005; Mo et al., 2002, 2009; Pan et al., 2012; Yin and Harrison, 2000). The plateau constitutes the thickest continental crust on Earth and numerous models are proposed for when it formed (e.g. Ji et al., 2009, 2012; Owens and Zandt, 1997). A key element in resolving the subduction and collision history of the India–Asia continents is to better understand the mantle nature beneath the plateau (e.g., Chu et al., 2006; Lee et al., 2009, 2012; Mo et al., 2005, 2008, 2009; Yin and Harrison, 2000). However, previous studies have focused on the petrology, geochronology and geochemistry of the giant Gangdese batholith and associated rocks (e.g., Linzizong volcanic sequence) in South Tibet (e.g., Aitchison and Davis, 2001; Aitchison

* Corresponding author at: Department of Earth Sciences, Sun Yat-Sen University, No. 135, Xingang Xi Road, Guangzhou 510275, China. Tel./fax: +86 20 841111209.
E-mail address: wangyuejun@mail.sysu.edu.cn (Y. Wang).

http://dx.doi.org/10.1016/j.lithos.2014.08.012
0024-4937/

et al., 2007; Cai et al., 2011; Chu et al., 2006; Chung et al., 2005; Lee et al., 2009, 2012; Mo et al., 2005, 2008, 2009; Wen et al., 2008a,b; Xie et al., 2011; Zhang et al., 2010a,b). The mafic components of these igneous rocks, potentially an important tracer of the mantle source beneath the Himalayan orogen and of Tethyan tectonic evolution, have received only limited study. Less attention has been paid to the early Eocene mafic rocks in SW Yunnan within the Tengchong fragment of the Sibumasu Block of the eastern Himalayan Syntaxis (e.g., Wang et al., 2014).

Our investigations in the Yinjiang and Longchuan areas of the Tengchong fragment identified small amounts of the Eocene amphibolite and metagabbroic rocks. These rocks provide new insight into the nature of the mantle source. Petrologic, zircon U–Pb and Lu–Hf isotopic data, along with whole-rock elemental and Sr–Nd isotopic compositions for the metabasites indicate that these mafic rocks crystallized at ~50–55 Ma and were metamorphosed at ~39 Ma. They show distinct geochemical signatures at different sites, but a consistent spatial variation from west to east, which resembles those in South Tibet (e.g., Zhao et al., 2011) and likely represents the southeastward continuation of the Gangdese magmatic belt in South Tibet (e.g., Ma et al., 2014; Wang et al., 2014).

2. Geological background and petrology

The Yinjiang–Longchuan region in SW Yunnan is wedge-shaped, tapering northward into the southeastern Himalayan Syntaxis and broadening southward into the Mogok metamorphic belt in Burma and NW Thailand (Fig. 1a, e.g., Morley et al., 2001; Wang et al., 2006; Yunnan BGMR, 1990). The region is assigned to the Tengchong fragment of the Sibumasu Block (e.g., Metcalfe, 1996, 1998; Wang et al., 2006).

The Tengchong fragment constituted part of Gondwana during the late Paleozoic that was accreted to Eurasia during the late Mesozoic (e.g., Morley et al., 2001; Wang, 1983). It has undergone strong Mesozoic and Cenozoic structural overprinting and is bounded by the Gaoligong dextral strike-slip fault to the east and the Sagaing fault to the west (e.g., Morley et al., 2001; Replumaz and Tapponnier, 2003; Wang et al., 2006). This fragment is composed mainly of pre-Mesozoic

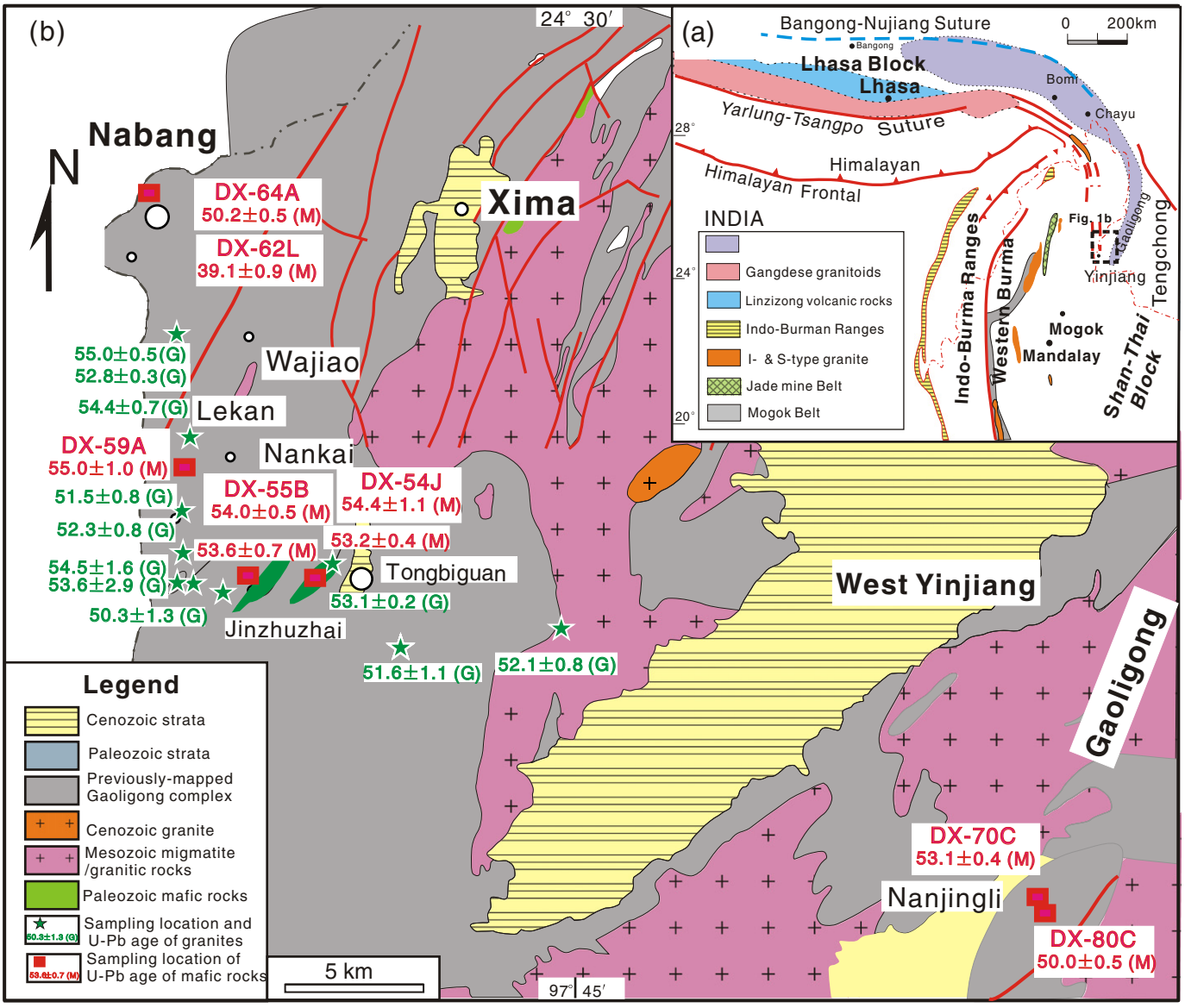

Fig. 1. (a) Schematic tectonic map of the Tibetan Plateau and SE Asia (modified after Chung et al., 2005 and Mitchell, 1993). (b) Geological map of the west Yinjiang area in SW Yunnan Province (revised from Wang et al., 2014). The square and pentangle symbols note the sampling locations and zircon U–Pb ages of the mafic and granitic rocks, respectively.

Table 1
Major oxides, elemental and Sr–Nd isotopic analytical results for early Eocene representative samples in the Tengchong fragment of Sibumasu.

	DX-62A	DX-62L	NB-6A	NB-6B	DX-64A	DX-63B	DX-59B	DX-55B	DX-54J	DX-78C	DX-78E	DX-80C	DX-80E	DX-80F	DX-80H
	Group 1				Group 2					Group 3					
	Nabang, west Yinjiang				Nabang, Yinjiang		Lekan	Jinzhuzhai	Tongbiguan	Nanjingli, Longchuan					
SiO_2	49.97	49.92	50.63	50.76	53.50	50.70	48.19	48.48	48.20	53.53	55.48	52.31	51.88	51.35	51.20
TiO_2	1.39	1.46	1.46	1.47	0.52	0.80	0.65	0.82	1.26	1.10	1.01	1.14	1.21	1.23	1.28
Al_2O_3	14.34	15.45	13.60	13.59	14.63	17.23	16.79	15.91	18.91	17.95	17.68	18.38	18.26	18.31	18.03
FeOt	11.75	10.31	14.23	14.35	7.95	9.10	11.16	11.54	10.52	7.51	6.97	9.75	9.41	9.38	9.87
MgO	7.70	6.53	6.28	6.33	7.33	6.24	9.23	7.87	5.45	5.05	4.56	4.21	4.76	4.87	5.07
CaO	11.16	11.64	10.60	10.78	9.62	9.17	10.32	10.63	9.23	7.88	6.94	6.85	7.08	7.65	7.34
K_2O	0.71	0.64	0.24	0.22	1.40	1.27	0.24	1.35	1.80	1.48	1.58	2.56	2.70	2.47	2.66
Na_2O	1.13	1.75	0.89	0.70	3.23	3.88	1.65	1.89	2.92	3.63	3.57	2.97	2.85	2.78	2.68
MnO	0.19	0.19	0.25	0.24	0.15	0.14	0.21	0.19	0.16	0.16	0.20	0.17	0.16	0.15	0.18
P_2O_5	0.08	0.16	0.14	0.13	0.35	0.51	0.24	0.08	0.35	0.29	0.27	0.47	0.48	0.44	0.42
LOI	1.11	1.53	1.54	1.27	0.88	0.48	0.77	0.77	0.73	0.97	1.29	0.71	0.74	0.91	0.82
Total	99.55	99.57	99.88	99.85	99.54	99.54	99.45	99.54	99.53	99.54	99.55	99.53	99.53	99.54	99.54
mg-number	57	56	47	47	65	58	63	58	51	57	57	46	50	51	51
Sc	43	39	45	41	28	27	30	32	25	29	25	23	25	27	28
V	356	290	351	324	202	246	290	327	235	213	183	224	232	253	272
Cr	188	284	89	58	232	147	24	72	22	85	67	10	16	17	18
Co	45	41	43	38	35	33	38	47	31	25	21	25	26	28	29
Ni	71	74	54	41	69	48	17	57	14	25	21	4	8	9	9
Ga	17	17	17	18	16	22	21	18	22	20	19	25	23	22	22
Rb	10.9	9.6	6.8	5.2	35.0	23.6	7.2	59.1	64.3	204.0	232.0	306.0	284.0	239.0	295.0
Sr	80.2	179	149	153	878	895	830	439	717	413	316	614	668	743	612
Y	32.6	31.6	36.2	34.3	18.7	22.8	17.6	20.9	30.3	33.2	44.8	34.5	28	28.6	29.8
Zr	61	103	88	86	63	67	48	52	180	129	126	165	182	245	186
Nb	3.01	4.03	4.24	3.49	4.34	4.09	2.75	5.34	12.6	15.7	18.5	21.4	21.3	15.5	16.7
Ba	52.5	57.8	12.1	6.39	591	410	28.2	123	510	193	156	540	587	684	583
La	4.01	6.19	8.70	5.82	28.30	31.30	14.10	13.10	32.60	24.60	22.10	28.30	25.60	23.20	23.60
Ce	9.59	12.90	19.30	13.80	57.20	68.20	27.70	28.80	69.30	48.80	46.00	67.90	57.10	59.30	59.70
Pr	1.46	1.88	2.71	1.94	6.87	8.30	3.45	3.75	8.73	5.95	5.59	8.98	7.33	8.35	8.30
Nd	7.47	9.94	13.20	10.10	28.60	35.20	14.70	15.70	34.80	24.30	23.30	38.70	31.60	35.40	36.00
Sm	2.62	3.34	3.89	3.56	6.25	7.48	3.43	3.66	7.20	5.55	5.49	8.77	7.04	8.04	7.98
Eu	1.01	1.25	1.28	1.25	1.58	1.96	1.14	1.00	1.82	1.52	1.54	1.98	1.78	2.18	2.13
Gd	3.99	4.81	4.85	4.65	5.55	6.43	3.50	3.88	6.77	5.37	5.79	7.51	6.20	6.90	7.45
Tb	0.76	0.80	1.02	0.94	0.69	0.87	0.56	0.59	0.96	0.86	1.02	1.12	0.99	1.00	1.03
Dy	5.21	5.18	6.91	6.66	3.46	4.12	3.01	3.41	5.47	4.95	6.18	6.13	5.18	4.95	5.43
Ho	1.21	1.20	1.40	1.35	0.70	0.82	0.67	0.77	1.14	1.12	1.49	1.27	1.08	1.06	1.12
Er	3.54	3.23	4.06	3.84	1.78	2.20	1.88	2.06	2.98	3.20	4.35	3.34	2.71	2.80	2.97
Tm	0.52	0.49	0.62	0.58	0.23	0.26	0.27	0.31	0.41	0.46	0.70	0.48	0.39	0.41	0.42
Yb	3.38	3.02	4.02	3.83	1.59	1.73	1.81	2.06	2.49	3.22	5.03	3.21	2.45	2.63	2.75
Lu	0.50	0.45	0.63	0.58	0.23	0.25	0.27	0.30	0.35	0.52	0.76	0.44	0.35	0.38	0.39
Hf	1.93	3.16	3.37	3.19	2.68	2.77	1.75	2.35	5.24	3.29	3.38	5.22	4.92	6.50	3.92
Ta	0.21	0.29	0.56	0.36	0.17	0.19	0.19	0.46	0.67	1.08	1.27	1.28	1.01	0.81	0.77
Pb	10.12	8.20	9.79	10.90	18.08	19.83	6.17	8.26	8.35	19.59	21.34	21.46	19.48	17.03	17.85
Th	0.77	0.90	1.15	0.77	2.37	2.22	4.06	3.21	3.79	8.10	9.79	8.76	7.36	6.24	6.15
U	0.58	0.40	0.46	0.47	0.61	0.35	1.15	1.28	0.70	5.01	5.91	5.02	3.43	4.22	2.61
$^{87}Rb/^{86}Sr$	0.393				0.115			0.389	0.259	1.429	2.125	1.442	1.230	0.931	1.395
$^{87}Sr/^{86}Sr$	0.707752				0.706450			0.705834	0.707751	0.709204	0.710917	0.710246	0.709842	0.709477	0.709904
2 σ	13				14			12	13	11	13	11	11	11	10
$(^{87}Sr/^{86}Sr)_i$	0.707529				0.706363			0.705541	0.707556	0.708128	0.709317	0.709160	0.708915	0.708776	0.708854
$^{147}Sm/^{144}Nd$	0.212				0.132			0.141	0.125	0.138	0.142	0.137	0.135	0.137	0.134
$^{143}Nd/^{144}Nd$	0.512940				0.512561			0.512534	0.512341	0.512263	0.512270	0.512228	0.512249	0.512271	0.512246
2 σ	9				8			10	8	9	9	8	8	9	8
$\varepsilon_{Nd}(t)$	5.8				−1.1			−1.7	−5.30	−6.9	−6.8	−7.6	−7.2	−6.7	−7.2

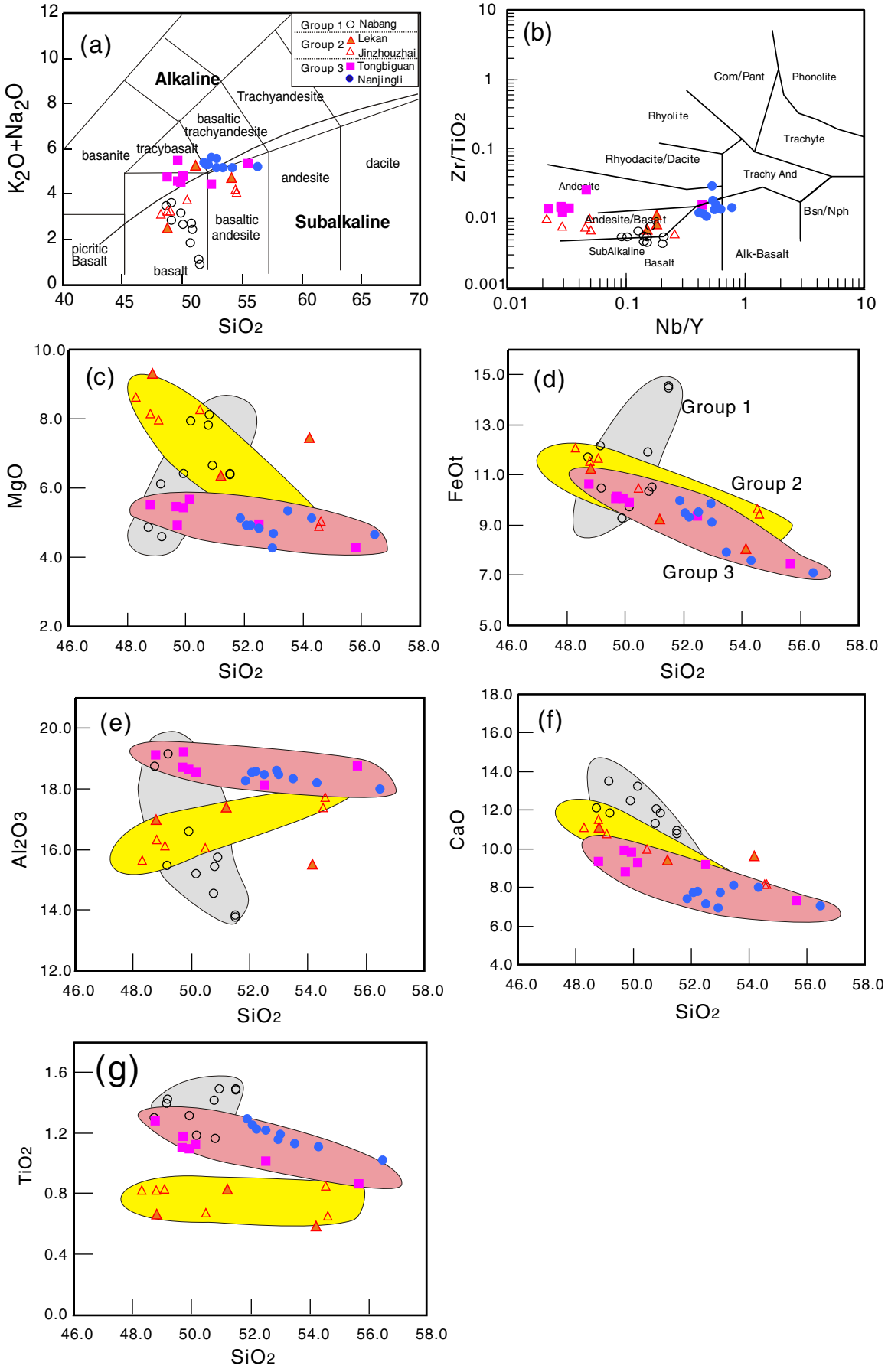

Fig. 2. (a) SiO_2 versus $K2O+Na_2O$; (b–f) Harker diagrams for the metabasic rocks in west Yinjiang area (SW Yunnan) of the Tengchong fragment. Symbols are the same as in Fig. 2a.

metamorphic rocks, Mesozoic–Tertiary granite and associated metapelite, metasandstone, slate and volcaniclastic rock (Fig. 1b; e.g., Yunnan BGMR, 1990). The low-grade metamorphic sequences consist of sandstone, shale, slate and limestone, along with interbanded glacial conglomerate and shale containing cold-water Gondwana-type fossil assemblages (e.g., Metcalfe, 1996, 1998; Ueno, 2000; Wang, 1983; Wu et al., 1995;

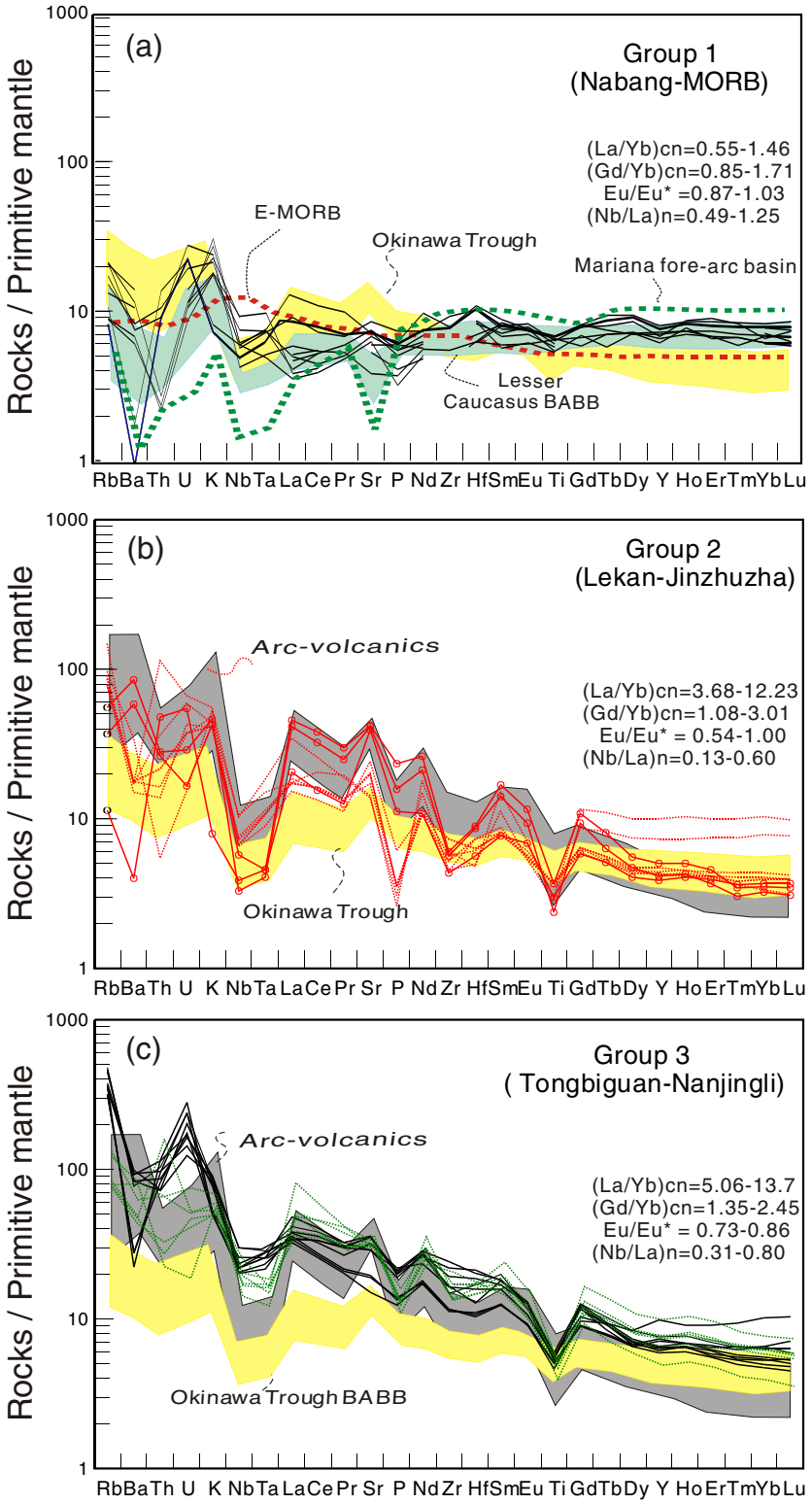

Fig. 3. Primitive mantle-normalized patterns of incompatible elements for the metabasic rocks of west Yinjiang area (SW Yunnan) of the Tengchong fragment. (a) Group 1 represented by the Nabang amphibolite, (b) Group 2 constituted by the mafic samples from Lekan and Jinzhouzhai, along with DX-62A and -62C from Nabang, (c) Group 3 composed of the metagabbroic and amphibolitic samples from the Tongbiguan and Nanjingli areas. Normalized values for primitive mantle are from Sun and McDonough (1989). Data for the Okinawa Trough back-arc basin basalt, fore-arc basin from Izu–Bonin–Mariana system and average Lesser Caucasus back-arc basin basalt are from Shinjo et al. (1999), Reagan et al. (2010), Pearce et al. (1995) and Rolland et al. (2009).
The values of N-MORB and E-MORB are after Sun and McDonough (1989).

Zhong, 1998). High-grade metamorphic rocks within the region are paragneiss, orthogneiss, leucogranite and migmatite with minor mafic–ultramafic fragments, which were previously inferred as the representative of the Tengchong Precambrian crystalline basement (e.g., Wang, 1983; Yunnan BGMR, 1990). Recent studies, however, have revealed that the gneiss, leucogranite and migmatite mainly crystallized during the Cretaceous and Cenozoic with ages clustering at ~140–70 Ma and ~50 Ma, and geochronologically resembling the Gangdese igneous belt in South Tibet (e.g., Ma et al., 2014; Peng et al., 2006; Song et al., 2010; Wang et al., 2006; Xu et al., 2012; Yang et al., 2002).

Along the China–Burma border and at Gaoligong Mountain, small amounts of mafic and ultramafic rocks are preserved in the gneisses as lenses, tectonic slices or dikes, and have experienced amphibolite- or granulite-facies metamorphism. The amphibolite and mafic granulite have been traditionally regarded as ophiolite relics related to the Neotethyan subduction (e.g., Ji et al., 2000a,b). In addition, several metagabbroic plutons and dikes have recently been identified (e.g., Tongbiguan plutons, Fig. 1b; Wang et al., 2014). We collected amphibolite samples from the Nabang and Nanjingli (Longchuan) areas and metagabbros from the Tongbiguan, Nabang, Lekan and Jinzhuzhai and Nanjingli areas (Fig. 1). The amphibolite displays blastoaplitic and blastoporphyritic textures. The mineral assemblage contains amphibole (~40–50% in volume), plagioclase (30–50%), and small amounts of sericite, clinozoisite, chlorite and magnetite. Amphibole is present as elongate crystals in a fine-grained plagioclase groundmass. The metagabbroic samples exhibit a medium- to coarse-grained igneous texture and contain clinopyroxene (~10–20%), amphibole (~25–40%), plagioclase (~30–50%), along with the accessory phases zircon, apatite, magnetite, ilmenite and titanite.

3. Analytical methods

During the sample preparation, any weathered rinds were removed prior to pulverizing to 200-mesh using an agate mill for elemental and isotopic analyses. Major oxides were measured by a wavelength X-ray fluorescence spectrometer using a Rigaku ZSX100e instrument at the Guangzhou Institute of Geochemistry (GIG), Chinese Academy of Sciences (CAS) with resultant analyses showing relative standard derivations of <5%. Trace element abundances were analyzed using a Perkin-Elmer Sciex ELAN 6000 inductively coupled plasma mass spectrometer (ICP-MS) at GIG, CAS. Detailed sample preparation and analytical procedure followed Wei et al. (2002). About 100 mg samples were digested with 1 ml of HF and 0.5 ml HNO_3 in screw top PTFE-line stainless steel bombs at 190 °C for 12 h. Insoluble residues were dissolved using 8 ml of 40% HNO_3 (v/v) heated to 110 °C for 3 h. Detailed sample preparation and chemical separation follows Wei et al. (2002). Sr–Nd isotope ratios were measured on a VG-354 mass-spectrometer at GIG, CAS and detailed sample analytical procedure follows Liang et al. (2003). The total procedure blanks were in the range of 200–500 pg for Sr and ≤50 pg for Nd. The mass fractionation corrections for Sr and Nd isotopic ratios are based on $^{86}Sr/^{88}Sr = 0.1194$ and $^{146}Nd/^{144}Nd = 0.7219$, respectively. The measured $^{87}Sr/^{86}Sr$ ratio of the (NIST) SRM 987 standard is 0.710265 ± 12 (2σ) and the $^{143}Nd/^{144}Nd$ ratio of the La Jolla standard is 0.511862 ± 10 (2σ). During the analytical process, within-run errors of precision are estimated to be better than 0.000015 for $^{146}Nd/^{144}Nd$ in the 95% confidence level. The elemental and isotopic analytical results of the samples are listed in Supplementary Dataset 1 and Table 1.

Zircon grains were separated using standard density and magnetic separation techniques, and then handpicked under a binocular microscope. The grains were mounted on adhesive tape, enclosed in epoxy resin, polished and coated with gold. Their internal texture was examined using cathodoluminescence (CL) imaging by a JXA-8100 scanning electron microprobe at GIG, CAS. The accelerating voltage of the microprobe was 15 kV and the sample current was 10 nA with a beam diameter ranging from 1 to 5 μm. The U–Pb and the Lu–Hf isotopic data for zircons from seven samples were performed on polished mounts using a Cameca 1280 large-radius SIMS at the Institute of Geology and Geophysics, CAS (DX-55B and DX-80C) and a Nu Plasma

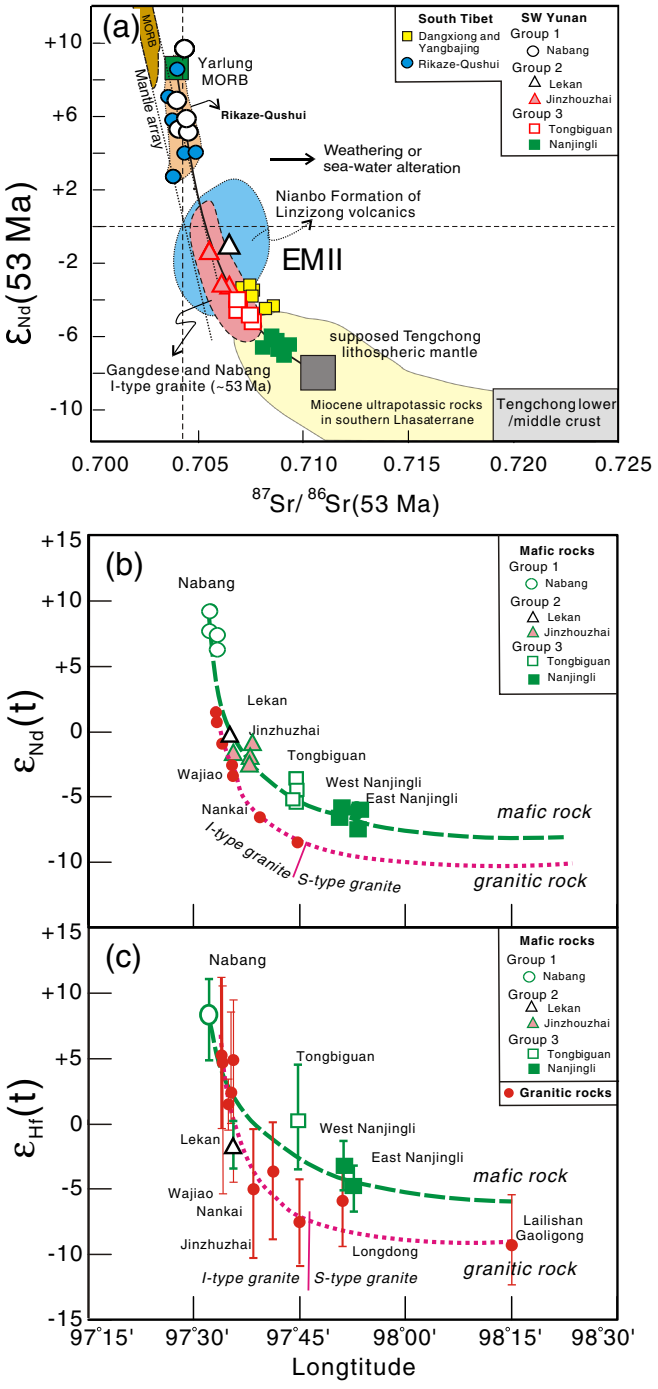

Fig. 4. (a) Initial Sr–Nd isotopic composition and (b–c) the spatial variation of whole-rock $\varepsilon_{Nd}(t)$ and zircon in-situ $\varepsilon_{Hf}(t)$ from the early Eocene mafic (dashed line) and granitic (dotted line) samples from Nabang across Jinzhuzhai–Tongbiguan onto Nanjingli and Lailishan in West Yingjiang of the Tengchong fragment. The granitic rocks to east and west of Tongbiguan are characterized by S- and I-type granitic rocks, respectively (e.g., Ma et al., 2014; Xu et al., 2012). Also shown in (a) are the data for the Yarlung MORB, supposed Tengchong/Yangtze lithospheric mantle, Tengchong lower/middle crust, Xigaze–Qushui, Dangxiong and Yangbajin gabbros and Miocene ultrapotassic rocks in South Tibet, the synchronous Gangdese and Nabang I-type granite and Nianbo volcanic rocks of the Linzizong sequence (e.g., Dong et al., 2005, 2006, 2008; Huang et al., 2010; Lee et al., 2009, 2012; Ma et al., 2014; Mo et al., 2009; Song et al., 2010; Wen et al., 2008a, 2008b; Xu et al., 2012; Zhu et al., 2009, 2011, 2012).
The data in (b) and (c) are from this study, Wang et al. (2014), Ma et al. (2014) and Xu et al. (2012).

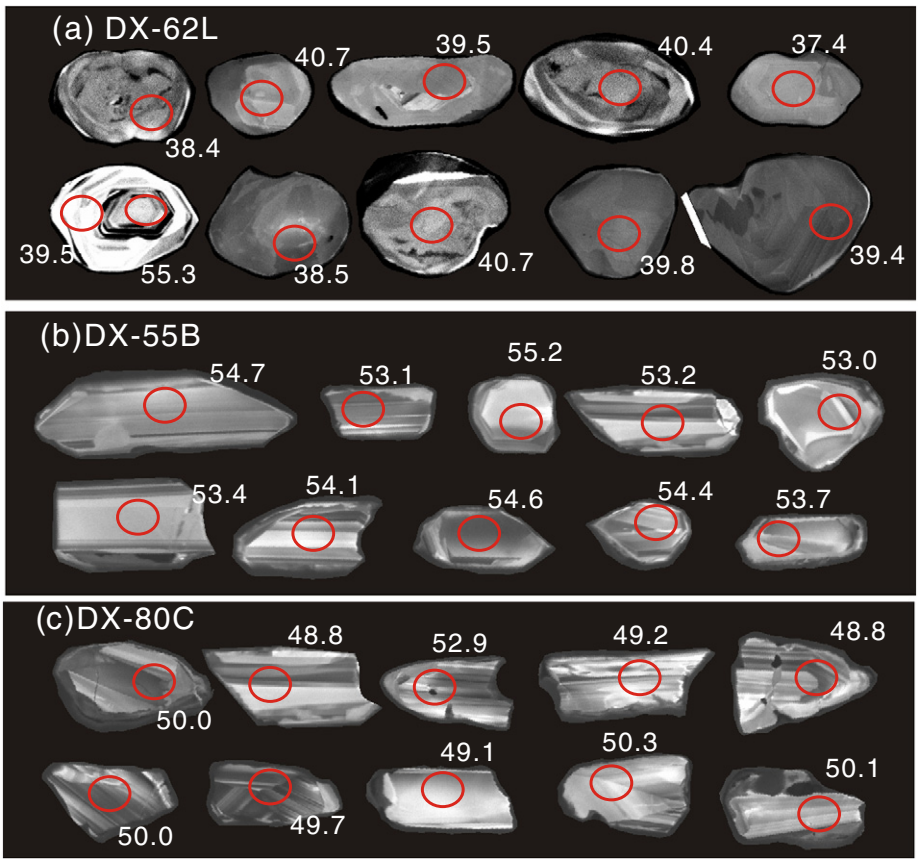

Fig. 5. CL images of representative zircons for Nabang amphibolite (DX-62L), and Jinzhuzhai and Nanjingli metagabbros (DX-55B and DX-80C), respectively.

MC-ICP-MS attached to the Resonetics M-50-HR Excimer Laser Ablation System at the Department of Earth Sciences, University of Hong Kong (DX-62L, DX-64A, DX-59, DX-54J and DX-78C), respectively. The instrumental setting and detailed analytical procedures for the SIMS dating techniques are described by Li et al. (2010a,b) and for the Lu–Hf ICP determinations by Xia et al. (2011). $^{207}Pb/^{206}Pb$ and $^{206}Pb/^{238}U$ ratios were calculated using GLITTER 4.0. Common Pb correction was made using the observed ^{204}Pb peak. The analytical results for zircon U–Pb and Lu–Hf isotopic compositions are listed in Supplementary Dataset 2.

4. Results

4.1. Geochemical characteristics

Our samples from the Nabang, Lekan, Jinzhouzhai, Tongbiguan and Nanjingli areas have SiO_2 = 48.14–56.46 wt.% (volatile-free), MgO = 3.30–8.51 wt.% and TiO_2 = 0.53–1.39 wt.%. They have variable K_2O and Na_2O+K_2O contents with Na_2O/K_2O = 1.05–3.18 (Supplementary Dataset 1). These samples are basalt and basaltic andesite (Middlemost, 1994) and can be classified, on the basis of their geochemical signatures (Fig. 2a–b), into three groups, named herein Groups 1, 2 and 3 (Figs. 2–4).

Group 1, consisting of the majority of samples from Nabang, shows positive correlations between SiO_2 and MgO and FeOt and negative correlations between SiO_2 and CaO and Al_2O_3 (Fig. 2c–f). The group has high TiO_2 but low P_2O_5 contents irrespective of SiO_2 (Fig. 2g), Group 2 is taken from Lekan and Jinzhouzhai, along with DX-62A and -62C from Nabang. This group exhibits a decrease in MgO, FeOt and CaO but increase in Al_2O_3, and relatively constant TiO_2 and P_2O_5 with increasing SiO_2 (Fig. 2c–g). Group 3 samples are composed of metagabbro and amphibolite from the Tongbiguan and Nanjingli areas. They show a negative correlation between SiO_2 and MgO, FeOt, CaO, TiO_2 and P_2O_5, but a positive correlation between MgO and Cr and Ni (Fig. 2). In comparison with Group 2, Group 3 shows lower MgO, FeOt, CaO, Cr and Ni, but higher Al_2O_3, TiO_2 and P_2O_5 at comparable SiO_2 or MgO (Fig. 2).

Table 2
Summary of sampling locations and zircon U–Pb and Lu–Hf analyses of the early Eocene mafic rocks.10DX-54B and 10DX-55E are from Wang et al. (2014).

Sample	Lithology	Sampling location	Zircon U–Pb age	Dating methods	$\varepsilon_{Hf}(t)$	Model age
DX-62L	Amphibolite	Nabang, west Yinjiang N 24°45.111′, E97°33.849′	39.1 ± 0.7 Ma, n = 27, MSWD = 1.6	LA-ICPMS	+5.1 to +11.6	0.28–0.52 Ga
			55.3 ± 2.1 Ma, n = 1		+11	0.27 Ga
DX-64A	Metagabbro	Nabang, west Yinjiang N 24°45.111′, E97°33.849′	50.2 ± 0.5 Ma, n = 22, MSWD = 0.7	LA-ICPMS		
DX-59	Metabasic rock	Lekan, west Yinjiang N 24°40.382′, E97°35.061′	55.0 ± 1.0 Ma, n = 13, MSWD = 2.2	LA-ICPMS	−4.6 to −0.9	0.75–0.89 Ga
DX-55B	Metagabbro	Jinzhuzhai, west Yinjiang N 24°36.498′, E97°34.996′	54.4 ± 1.1 Ma, n = 13, MSWD = 1.1	SIMS		
10DX-55E	Metagabbro	Jinzhuzhai, west Yinjiang N 24°36.498′, E97°34.996′	53.6 ± 0.7 Ma, n = 23, MSWD = 6.1	LA-ICPMS		
10DX-54B	Metagabbro	Tongbiguan, west Yinjiang N 24°37.514′, E97°37.764′	53.2 ± 0.4 Ma, n = 30, MSWD = 3.6	LA-ICPMS	−3.1 to +2.9	0.53–0.84 Ga
DX-54J	Metagabbro	Tongbiguan, west Yinjiang N 24°37.514′, E97°37.764′	54.0 ± 0.5 Ma, n = 16, MSWD = 0.7	LA-ICPMS		
DX-78C	Metagabbro	West Nanjingli, Longchuan N 24°07.465′, E97°49.543′	53.1 ± 0.4 Ma, n = 23, MSWD = 1.3	LA-ICPMS	−5.1 to −2.2	0.79–0.92 Ga
DX-80C	Metagabbro	East Nanjingli, Longchuan N 24°05.841′, E97°50.720′	50.1 ± 0.6 Ma, n = 15, MSWD = 1.5	SIMS	−7.1 to −4.1	0.89–1.01 Ga

Group 1 samples show relatively flat chondrite-normalized REE patterns with insignificant Eu anomalies (Supplementary Dataset 1). In Fig. 3a, Group 1 samples are marked by subparallel and slightly-left sloping primitive mantle (PM)-normalized patterns with the exception of Rb, Ba, Th, U and K. Such patterns are generally similar to those of the Okinawa Trough continental back-arc basin basalt (BABB) from Rb to La and identical to those of the Lesser Caucasus BABB from Nd to Lu (Fig. 3a). Their (Nb/La)n, (Hf/Sm)n and (Th/La)n (Supplementary Dataset 1) resemble those of the Okinawa Trough continental BABB. Group 2 has high (La/Yb)cn and (Gd/Yb)cn and slightly negative Eu anomalies and exhibits subparallel spiky patterns with enrichment in LILEs and depletion in HFSEs, together with sharply negative Nb–Ta, Zr–Hf and P–Ti anomalies (Fig. 3b). The (Nb/La)n values for Group 2 range from 0.13 to 0.60 with the majority being at ~0.30 and (Th/La)n from 0.44 to 0.97. Their PM-normalized patterns are similar to those of arc volcanics and the Dangxiong gabbroic and Yangbajin ultrapotassic rocks in South Tibet (Fig. 3b; e.g., Gao et al., 2010; Luhr and Haldar, 2006; Pearce et al., 1995; Tommasini et al., 2011; Zhao et al., 2011). Group 3 samples have higher LREEs and incompatible elemental contents in comparison with Groups 1 and 2 (Supplementary Dataset 1 and Table 1). They show steeper REE- and PM-normalized patterns with negative Nb–Ta anomalies and insignificant Zr–Hf and P depletion (Fig. 3c), along with high (La/Yb)cn and (Gd/Yb)cn and weakly negative Eu anomalies. Their (Nb/La)n ratios range from 0.31 to 0.80.

The initial Sr isotopic ratios for Group 1 vary from 0.7041 to 0.7046 and the $\varepsilon_{Nd}(t)$ values range from +5.3 to +9.5 (Table 1), similar to those of MORB and the ~52 Ma Rikaze–Qushui mafic rocks in South Tibet (Fig. 4a; e.g., Dong et al., 2005, 2006, 2008). Group 2 shows $^{87}Sr/^{86}Sr(t)$ of 0.7055–0.7066 and $\varepsilon_{Nd}(t)$ of −1.1 ~ −3.6, which are slightly higher than those of the synchronous Dangxiong and Yangbajin gabbros in South Tibet (e.g., Gao et al., 2010; Zhao et al., 2011), and plot in the range of the Nianbo volcanic rocks of the Linzizong sequence (Fig. 4a, e.g., Lee et al., 2012; Mo et al., 2009; Zhu et al., 2009, 2011, 2012 and references therein). Group 3 has an affinity to an EM2-like source with $^{87}Sr/^{86}Sr(t)$ ranging from 0.7070 to 0.7093 and $\varepsilon_{Nd}(t)$ from −4.3 to −7.6, and is close to those of the Tengchong and Yangtze lithospheric mantle, and falling into the field of the Miocene ultrapotassic rocks in South Lhasa. Sr–Nd isotopic compositions for the three groups plot along the mantle array between the Yarlung MORB and supposed Tengchong lithospheric mantle (Fig. 4a; e.g., Hart, 1984, 1988; Hofmann, 1997; Wang et al., 2014).

4.2. Zircon U–Pb and Lu–Hf systematics

The CL images of representative grains from DX-62L (Group 1), DX-55B (Group 2) and DX-80C (Group 3) are shown in Fig. 5a–c. Sampling locations along with a summary of zircon U–Pb dating and Lu–Hf analytical results are shown in Fig. 1 and Table 2. The corresponding concordia diagrams for the seven samples are given in Fig. 6.

DX-62L is an amphibolite from Nabang, west Yinjiang in SW Yunnan, representative of Group 1. Only one grain (DX-62L-30) exhibits an oscillatory zoned core and metamorphic rim, with the core giving a $^{206}Pb/^{238}U$ apparent age of 55.3 ± 2.1 Ma and the bright rim yielding a $^{206}Pb/^{238}U$ apparent age of 39.5 ± 1.4 Ma (Supplementary Dataset 2 and Table 2). The remaining grains display poor zonation without core (Fig. 5a) and are considered to be of metamorphic origin. These grains have Th/U ratios of 0.78–1.48 and form an age-cluster with a weighted mean age of 39.1 ± 0.7 Ma with MSWD = 1.6 (n = 27, Fig. 6a). In combination with CL imaging, 55.3 Ma is taken as the igneous crystallization age of the sample and 39.1 Ma as the timing of metamorphism (Fig. 6a). The corresponding $\varepsilon_{Hf}(t)$ value for the igneous core is +11 and those for the metamorphic grains range from +5.1 to +11.6 with the Hf model age of 0.52–0.25 Ga.

DX-64A, DX-59 and DX-55B, representative of Group 2, are metagabbroic rocks taken from Nabang, Lekan and Jinzhuzhai, respectively (Fig. 1 and Table 2). Zircons from these samples are largely subhedral, light-brown to colorless crystal grains or fragments and exhibit weak oscillatory zoning with variable luminescence in the CL images, indicative of an igneous origin (Fig. 5b). Twenty-two grains from DX-64A have Th/U ratios of 0.50–1.60 and $^{206}Pb/^{238}U$ apparent ages of 52.8 Ma to 48.3 Ma with a weighted mean age of 50.2 ± 0.5 Ma (MSWD = 0.7; Fig. 6b). Thirteen analyses on 13 grains for DX-59 give a weighted mean age of 55.0 ± 1.0 Ma (MSWD = 2.2, Fig. 6c) with corresponding $\varepsilon_{Hf}(t)$ values of −4.6 to −0.9 and T^{Hf}_{DM} range of 0.89 to 0.75 Ga. The zircons from DX-55B have Th/U ratios of 0.12–0.71 and weighted mean ages of 54.0 ± 0.5 Ma (n = 16, MSWD = 0.7; Fig. 6d), identical within error of the age of 53.6 ± 0.7 Ma reported by Wang et al. (2014).

The DX-54J metagabbro and DX-78C and DX-80C amphibolites were collected from Tongbiguan and Nanjingli (Longchuan) and are representative of Group 3 (Fig. 1 and Table 2). The zircons from DX-54J have Th/U ratios ranging from 0.47 to 1.52, and a weighted mean age of 54.4 ± 1.1 Ma (n = 13, MSWD = 1.5, Fig. 6e). The separated zircons from DX-78C and DX-80C show the variable Th/U ratios of 0.14–2.19 (Supplementary Dataset 2) and oscillatory zoning of magmatic grains (Fig. 5c). Two samples yield weighted mean $^{206}Pb/^{238}U$ ages of 53.1 ± 0.4 Ma (DX-78C, n = 23, MSWD = 1.3) and 50.0 ± 0.5 Ma (DX-80C, n = 14, MSWD = 0.7, Fig. 6f–g). Their $\varepsilon_{Hf}(t)$ values range from −5.1 to −2.0 for DX-78C and −7.2 to −4.1 for DX-80C and corresponding T_{DM} values from 0.92 Ga to 0.79 Ga and 1.01 Ga to 0.89 Ga, respectively (Supplementary Dataset 2 and Table 2).

5. Discussion

The low Mg-number and Ni and Cr contents for the three groups indicate the fractional crystallization of olivine and clinopyroxene during magma evolution. However, the distinct REE and trace element patterns, Nb/La ratios and Sr–Nd isotopic compositions (Figs. 3–4) indicate controls on the final rock composition beyond the simple fractionation process.

For the Group 1 samples, highly positive $\varepsilon_{Nd}(t)$ and $\varepsilon_{Hf}(t)$ values and high Nb/La but low Nb/Zr and Th/Zr argue for affinity to a MORB-like source. However, in comparison with an N-MORB source, these samples have higher contents of highly incompatible elements (e.g., Rb, Ba, Th, Nb, La and Ce) but similar contents of moderately incompatible elements (e.g., Tb, Dy, Y, Yb and Lu). They have higher Th and U contents and Th/Yb ratios than those of typical N-MORB (e.g., Sun and McDonough, 1989). Their Th/La ratios range from 0.07 to 0.19, falling between the bulk continental crust/arc volcanic rocks and N-MORB (e.g., Sun and McDonough, 1989). In addition, Group 1 has high Nb/La and Th/Yb and low Nb/Th ratios, and the majority of analyses fall to the left of the MORB–OIB array in the plot of Th/Yb and Nb/Yb (Fig. 7a). These characteristics of Group 1, together with linear correlations between (La/Sm)n vs (La/Nb)n and (Ta/Nb)n (Fig. 7b–c), as well as incompatible elemental patterns similar to back-arc basin basalt (Fig. 3a), indicate input of an arc component into a MORB source via subduction (see also Fig. 8e–g). In plots of Nd/Pb and Nb/Y ratios and isotopic compositions (Fig. 8a–b), Group 1 exhibits higher Nb/Y but lower Nd/Pb and slightly lower $\varepsilon_{Nd}(t)$ values than those of typical MORB mantle, suggesting the addition of the slab-derived fluid into the source. In Fig. 4a, these samples plot along the mixing line between depleted mantle and the supposed Tengchong crust or lithospheric mantle (e.g., Wang et al., 2014). Modeling results based on the SiO_2 and Sr–Nd isotopic compositions (Fig. 9a–b) show that the addition of 0.5–2.0% of a dehydrated sediment-derived component into a MORB source is required to explain the isotopic variations for Group 1. MgO and FeOt correlate positively but CaO and Al_2O_3 negatively with SiO_2 for the Group 1 samples, also suggestive of the minor involvement of a recycled sedimentary component that could induce the formation of the high Al_2O_3 and low FeOt magma source. Thus, these data suggest the derivation of Group 1 compositions from a MORB-like source

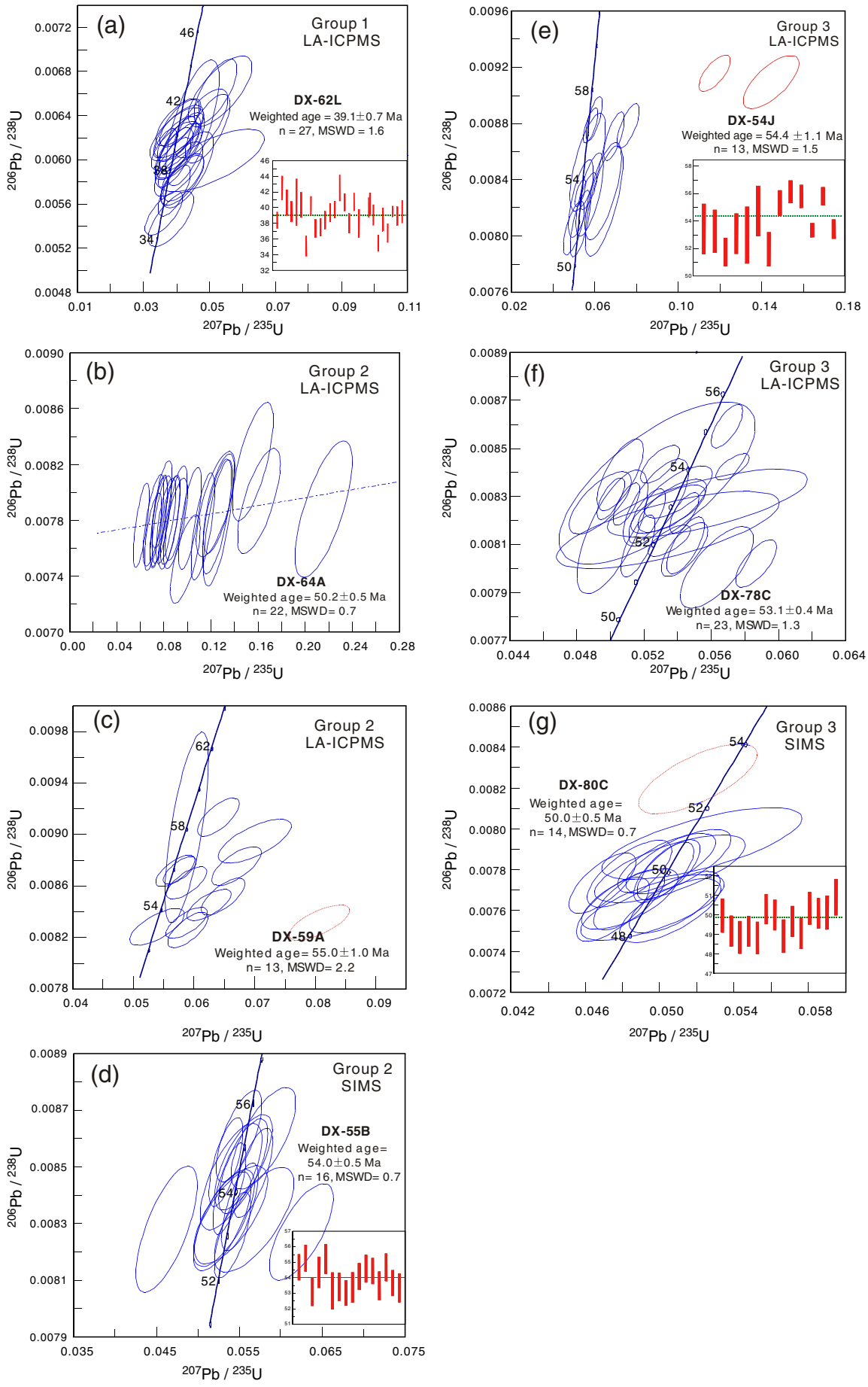
(a)
Group 1
LA-ICPMS
DX-62L
Weighted age = 39.1±0.7 Ma
n = 27, MSWD = 1.6
(b)
Group 2
LA-ICPMS
DX-64A
Weighted age= 50.2±0.5 Ma
n= 22, MSWD= 0.7
(c)
Group 2
LA-ICPMS
DX-59A
Weighted age= 55.0±1.0 Ma
n= 13, MSWD= 2.2
(d)
Group 2
SIMS
DX-55B
Weighted age=
54.0±0.5 Ma
n= 16, MSWD= 0.7
(e)
Group 3
LA-ICPMS
DX-54J
Weighted age = 54.4 ±1.1 Ma
n= 13, MSWD = 1.5
(f)
Group 3
LA-ICPMS
DX-78C
Weighted age= 53.1±0.4 Ma
n= 23, MSWD= 1.3
(g)
Group 3
SIMS
DX-80C
Weighted age=
50.0±0.5 Ma
n= 14, MSWD= 0.7
206Pb / 238U
207Pb / 235U

newly modified by slab- and sediment-derived components (e.g., Pearce and Peate, 1995; Shinjo et al., 1999).

A supra-subduction zone source for Group 1 rocks could occupy fore-arc (e.g., Isu–Bonin) or back-arc (e.g., Okinawa Trough, Lesser Caucasus, Kuertu and NW Hearne) basin settings (e.g., Bédard et al., 2009; Bezard et al., 2011; Hébert et al., 2012; Reagan et al., 2010; Sandeman et al., 2006; Shinjo et al., 1999). Fore-arc lavas have generally lower Ti/V and Yb/V ratios relative to the back-arc lavas and are commonly contemporaneous with boninite, high-Mg andesite and normal andesite, as documented in the Izu–Bonin–Mariana system (e.g., Reagan et al., 2010; Rolland et al., 2009; Shinjo et al., 1999). However, Group 1 samples have higher TiO_2 and Yb contents at comparable V contents and resemble those of Mariana BABB rather than fore-arc lavas (Table 1). The majority of the Group 1 samples have (La/Yb)n ranging from 0.54 to 1.46 and Sm/Nd from 0.31 to 0.44. These signatures, together with Th/Yb and Th/Nb ratios and REE and multi-elemental patterns, are partly identical to those of the Lesser Caucasus and Okinawa Trough BABB as well as the Cretaceous–Paleocene Rikaze–Qushui mafic rocks that are considered to have been generated in the back-arc basin setting (Fig. 3a, Bezard et al., 2011; Dong et al., 2008; Hébert et al., 2012; Hickey-Vargas, 1998; Reagan et al., 2010; Rolland et al., 2009; Shinjo et al., 1999). In addition, in the Nabang area, no boninite and high-mg andesite rocks have been identified. In summary, Group 1 was likely derived from a MORB-like source with a proportional input of a recycled component, probably in a back-arc basin setting.

For Group 2, the involvement of crustal components is marked by negative $\varepsilon_{Nd}(t)$ values (−1.1 ~ −3.6), high Al_2O_3 content (14.3–17.4 wt.%), enrichment in LILEs and depletion in HFSEs (e.g., Nb–Ta and Zr–Hf, Figs. 3b and 4a). Analyzed samples show high Ba/Nb and Th/Yb and low Nb/La, Nb/Th and Ce/Pb ratios, similar to those of typical arc magma and the synchronous Nianbo volcanic rocks in the Linzizong sequence and Dangxiong gabbro (Fig. 7a–c; e.g., Dong et al., 2006, 2008; Gao et al., 2008, 2010; Köhler et al., 2009; Lee et al., 2009, 2012; Luhr and Haldar, 2006; Mo et al., 2007; Nelson, 1992; Pearce and Cann, 1973; Pearce et al., 1984, 1995; Yue and Ding, 2006; Zhao et al., 2011). Such signatures indicate that Group 2 magma originated from (1) the mantle wedge newly modified by subducted sediments, or (2) the enriched lithospheric mantle with input of slab-derived fluid/melt. Our samples exhibit Th/La = 0.04–0.40, Ce/Pb = 3.0–5.9, Th/Yb = 0.27–2.50, Sr/La = 12–58 and Th/Nb = 0.48–1.90, contrary to what would be expected for a source metasomatized by the subducted Th-rich sedimentary component (e.g., Conticelli et al., 2009; Plank, 2005; Tommasini et al., 2011). In the plots of Nd/Pb, $^{87}Sr/^{86}Sr(t)$ and $\varepsilon_{Nd}(t)$ (Figs. 8b and 9b), Group 2 falls away from the mixing line involving depleted mantle and a subducted sedimentary component. In addition, modeling calculations show that 15–25% of the recycled sedimentary component is required to be added into the depleted mantle in order to match SiO_2 and Nd isotopic ratios (Fig. 9a). However, such a proportional addition cannot reconcile the Sr isotopic component and the abovementioned significant fractionation (Fig. 9b). Our data show Group 1 with a MORB-like source spatially developed at Nabang to west of the Lekan–Tongbiguan area where the Group 2 samples have an arc geochemical affinity. Such spatial variation suggests the eastward subduction of the Neotethyan Ocean in the Tengchong fragment (e.g., Ma et al., 2014; Wang et al., 2014). As shown in Table 1 and Fig. 4b–c, the Group 2 samples exhibit sharply decreasing $\varepsilon_{Nd}(t)$ and $\varepsilon_{Hf}(t)$ values from west (Nabang and Lekan) to east (Tongbiguan). This indicates a significantly increasing proportion of recycled sediments in the depleted mantle source for Group 2 from west to east when the above-mentioned case (1) has been considered. Such a trend is in contradiction with what would be expected for the transportation of the recycled sedimentary components into the source proportionally being lowered with the increasing distance to the suture

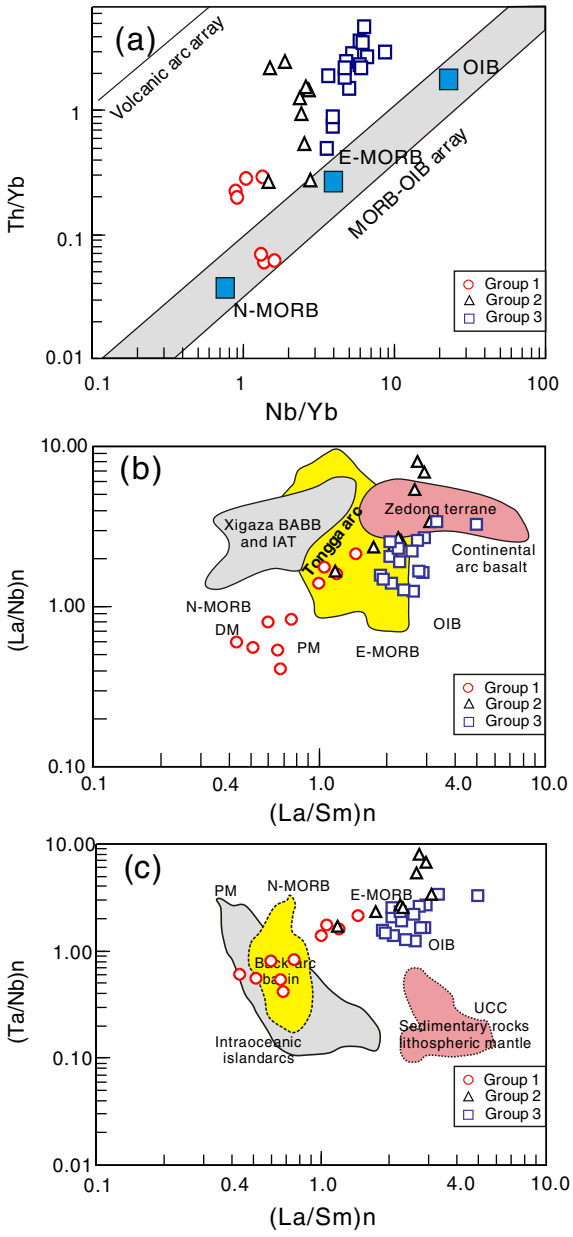

Fig. 7. (a) Nb/Yb vs Th/Nb, (b) (La/Sm)n vs (La/Nb)n and (c) (La/Sm)n vs (Ta/Nb)n for the metabasic rocks in SW Yunnan of the Tengchong fragment.

during the Neotethyan eastward subduction. In contrast, the Group 2 samples plot along the mixing line of slab-derived component and the preexisting Tengchong/Yangtze lithospheric mantle (Fig. 8a–b). A 13–20% input of the slab-derived component into the Tengchong lithospheric mantle could match the observed Sr–Nd isotopic ratios and explain the variations of the major oxides (Fig. 9a–b). The Nd–Hf isotopic variations in Table 1 and Fig. 4b–c for Group 2 from west to east could be reasonably interpreted as the result of the decreasing input of slab-derived fluid/melt into the enriched mantle from Lekan to Tongbiguan. Thus, an alternative scenario is that Group 2 can be petrogenetically attributed to the new input of the slab-derived component into the preexisting lithospheric mantle. Such an origin for Group 2 is comparable with those observed in the intracontinental BABB or arc setting (e.g., Sandeman et al., 2006). However, as shown in Fig. 3b, the REE and multi-elemental patterns of the Group 2 samples are subparallel to those of the island-arc basalts and Barren high-Al basalts rather than

Fig. 6. Zircon U–Pb concordia diagrams for the (a) Nabang amphibolite (DX-62L), (b, c) Nabang and Lekan metagabbroic rocks (DX-64A and DX-59) and (d, e) Jinzhuzhai (DX-55B) and Tongbiguan (DX-54J) metagabbroic rocks, along with (f, g) amphibolite samples from west and east Nanjingli (DX-78C and DX-80C), respectively.

those of the Okinawa BABB (e.g., Luhr and Haldar, 2006; Pearce and Cann, 1973; Pearce et al., 1984, 1995). On the plots of Ti–Zr, La/Nb–Nb/Th, Th–Ta–Hf, Zr–Y–Nb and Zr–Y–Ti (Fig. 8c–g), Group 2 falls mainly in the field of volcanic arc basalts (e.g., Dilek et al., 2008; Reagan et al., 2010). These data, together with the negative $\varepsilon_{Nd}(t)$ and $\varepsilon_{Hf}(t)$ values, indicate that Group 2 formed in an early Eocene continental arc setting.

In comparison with Group 2, Group 3 samples have higher contents of highly incompatible elements but similar moderately incompatible elemental contents. Their elemental patterns resemble arc volcanic rocks (Fig. 3c). The $\varepsilon_{Nd}(t)$ values range from −4.3 to −7.6, with which of the Tongbiguan samples being slightly higher than the Dangxiong and Yangbajing mafic rocks, and of Nanjingli samples falling into the most depleted range of the Miocene ultrapotassic rocks in the South Lhasa terrane and near to the supposed Tengchong/Yangtze Blocks (Fig. 4a). In $\varepsilon_{Nd}(t)$ vs Nb/Y and Nd/Pb diagrams, these samples plot along the mixing line of the inferred Tengchong lithospheric mantle and slab-derived component but near to the Tengchong lithospheric end-member (Fig. 8a–b). Group 3 occurs in the Nanjingli area, spatially further away from the inferred Neotethyan subduction boundary than Group 2. Their $\varepsilon_{Nd}(t)$ and $\varepsilon_{Hf}(t)$ values are similar to those of the Northern magmatic belt of South Tibet (e.g., Debon et al., 1986; Harris et al., 1988; Huang et al., 2010) and show slightly decreasing trends in spite of the spatial locations being further eastward within the East Tengchong fragment relative to the other groups (e.g., Fig. 4b–c). Group 3 samples show similar multi-elemental pattern to typical arc volcanic rocks but generally higher contents of incompatible elements (Fig. 3c). They have slightly high Zr, Th and TiO_2 contents and Zr/Y and Th/Hf ratios in comparison to typical arc volcanic rocks and fall into the field of arc volcanics or the boundary of arc and within-plate basalt in Fig. 8d–g. The synthesis of these data suggests that Group 3 at Nanjingli probably originated from an enriched mantle with limited involvement of a recycled component and generated in an arc setting

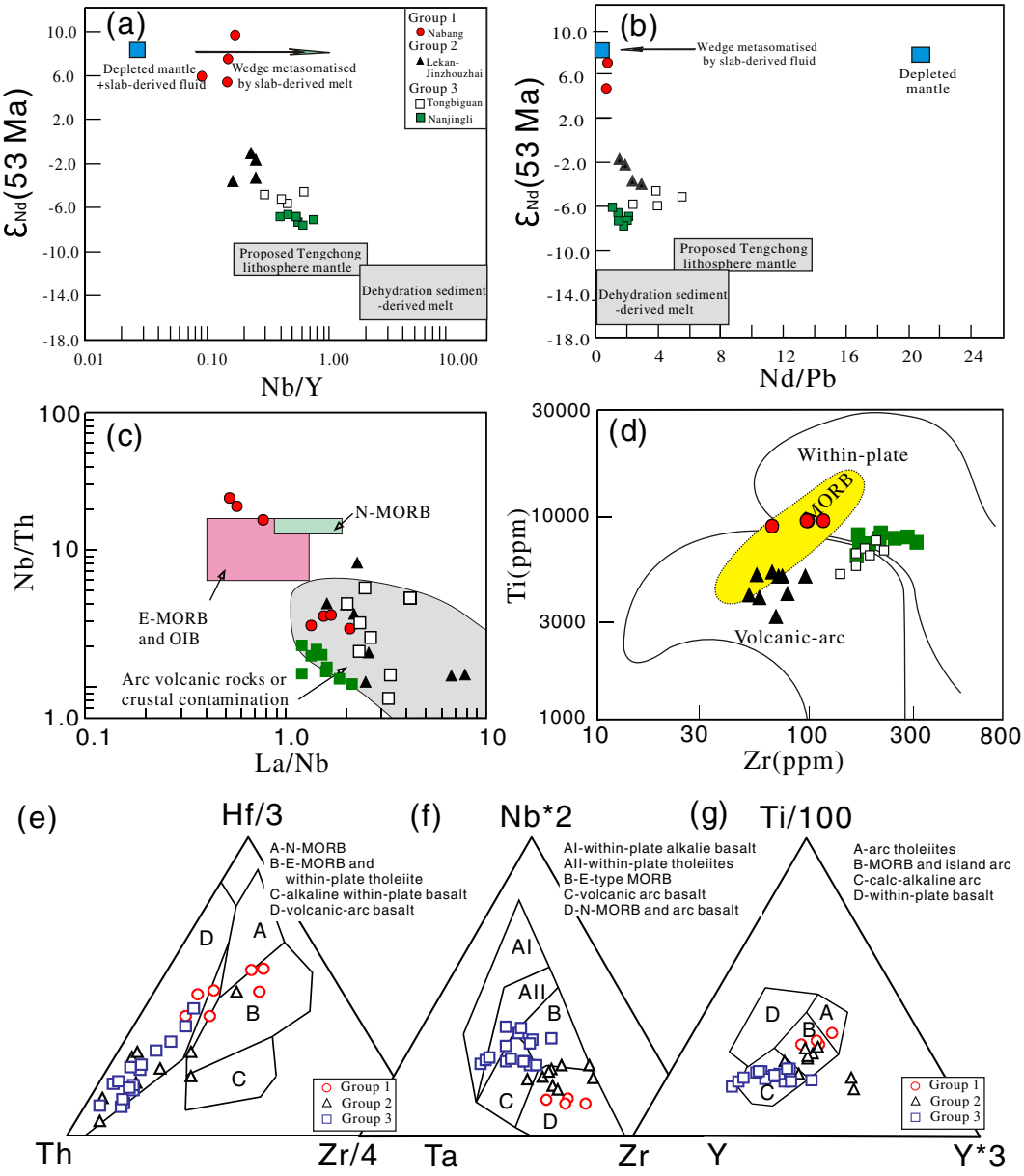

Fig. 8. $\varepsilon_{Nd}(t)$ vs Nb/Y (a) and Nd/Pb (b) for the mafic rocks in SW Yunnan of the Tengchong fragment. The compositions of the end-members are from Elliott et al. (1997), Class et al. (2000), Petrone and Ferrari (2008), Castillo et al. (2002, 2007) and Wang et al. (2013). These combined Nd/Pb and Nb/Y ratios with isotope compositions can effectively evaluate the nature of subduction components since Th, Nd, Nb and Y are fluid-immobile and dominated by sediment- and slab-derived melt, whereas Pb contribution is mainly controlled by fluid. (c–g) La/Nb–Nb/Th, Zr–Ti, Th–Ta–Hf, Zr–Y–Nb and Zr–Y*3-Ti/100 diagrams (after Wood, 1980; Meschede, 1986) for the mafic rocks in west Yinjiang (SW Yunnan) of the Tengchong fragment, respectively.

but nearby a within-plate environment. The modeling results in Fig. 9a–b also show the proportional (5–10%) involvement of the slab-derived component into the Tengchong lithospheric mantle.

6. Tectonic implications

The Gangdese batholith represents a major Cretaceous–Paleogene magmatic arc extending some 1500 km along southern Tibet that formed during the closure of the Neotethyan Ocean. At around ~52 Ma it displays a major magmatic flare-up, which is also expressed through the accumulation of the 5-km-thick Linzizong volcanic sequence (and associated minor mafic plutons) that lie to the south of the batholith (e.g., Aitchison et al., 2002; Chu et al., 2006, 2011; Chung et al., 2005; Dong et al., 2008; Lee et al., 2009, 2012; Mo et al., 2005, 2007, 2008, 2009; Searle et al., 1987; Yin and Harrison, 2000; Zhao et al., 2011; Zhu et al., 2009, 2011, 2012). How, or if, this magmatic pulse extends southeastward beyond the eastern Himalayan Syntaxis into NW Yunnan has not previously been resolved.

Our mafic rocks from Nabang–Nanjingli (west Yinjiang, NW Yunnan) yielded zircon U–Pb ages ranging from 55.3 Ma to 50.1 Ma. This age range is synchronous with that of granitic rocks from the Tengchong fragment (Ma et al., 2014; Song et al., 2010; Wang et al., 2014; Xu et al., 2012). Groups 1 and 2 are geochemically similar to those of the Yarlung–Rikaze–Qushui mafic rocks and Nianbo mafic rocks, respectively. The Sr–Nd–Hf isotopic compositions for Group 3 are generally similar to the Dangxiong–Yangbajing or the depleted component of the Cenozoic ultrapotassic rocks in South Tibet, along with the Tengchong/Yangtze lithospheric mantle (Fig. 6a; e.g., Dong et al., 2008; Zhao et al., 2011). Their Nd–Hf isotopic compositions show a pronounced decrease from west to east, extending from Group 1 at Nabang to Group 2 at Lekan–Jinzhouzhai, and then a less marked decrease further eastward to Group 3 at Tongbiguan–Nanjingli (Fig. 4b–c). Such a pattern is spatially comparable to that of the Cenozoic igneous rocks in South Tibet (e.g., Zhao et al., 2011).

Ma et al. (2014) recently reported the presence of early Eocene I-type gneissic granites at the Nabang–Tongbiguan area, which they interpreted to be derived from crustal materials modified by underplated juvenile basaltic magma. At the Tongbiguan–Gaoligong area of the eastern Tengchong fragment, the late Cretaceous–Paleogene (~120–50 Ma) S-type granites show strongly negative $\varepsilon_{Nd}(t)$ and $\varepsilon_{Hf}(t)$ values, and were interpreted as the product of melting ancient meta-sedimentary rocks (e.g., Xu et al., 2012). These data reveal a contrasting lithological and Nd–Hf isotopic variation from Nabang across Tongbiguan and onto Gaoligong of the Tengchong Block, with an abrupt change at Tongbiguan (Figs. 1a and 4b–c). This spatial trend is identical with that displayed by the igneous belt in the Lhasa Block involving the I-type Southern Gangdese and S-type Northern magmatic zones, respectively (e.g., Chiu et al., 2009; Chung et al., 2005; Harris et al., 1990; Huang et al., 2010; Kapp et al., 2005; Lee et al., 2009, 2012; Zhu et al., 2009, 2011, 2012 and reference therein). As a result, granitic and mafic rocks in the Nabang–Nanjingli region of SW Yunnan geochronologically and geochemically resemble the Gangdese magmatic belt in South Tibet (e.g., Dong et al., 2008; Zhao et al., 2011). The early Eocene magmatism in NW Yunnan is comparable with that of the Gangdese belt prior to the Indo-Asia collision, and thus should represent the eastward continuation of the Gangdese magmatic belt (e.g., Barley et al., 2003).

The timing of the initial collision of India with Asia is uncertain with suggestions ranging from ~65 Ma to 34 Ma (e.g., Aitchison et al., 2007; Hu et al., 2012; Jaeger et al., 1989; Klootwijk et al., 1992; Leech et al., 2005; Ma et al., 2014; Mo et al., 2002, 2008; Najman et al., 2010; Rowley, 1996; Wang et al., 2014; Yin, 2006; Yin and Harrison, 2000). The arc regime of the Eocene (55–50 Ma) mafic rocks in SW Yunnan is consistent with subduction still ongoing at this time. In detail, Groups 1 and 2 originated from MORB-like and preexisting lithospheric sources, respectively with input of a newly recycled component. Group 3 was derived from an enriched mantle with proportional involvement of a slab-derived component. Such an origin for Groups 2 and 3, in combination with the spatial distribution of the three groups, indicates a sharp decrease in the contribution of the slab-derived component and tectonic transformation of back-arc basin to continent margin, from west (Lekan) to east (Nanjingli), in the Tengchong fragment of the Sibumasu Block. Such a pattern suggests an easterly-directed subduction in response to the closure of the Neotethyan Ocean. In South Tibet, the marine sedimentation continued until ~50 Ma (e.g., Dewey et al., 1988; Gaetani and Gaetani, 1991; Hodges, 2000; Rowley, 1996) and the early Cenozoic (~66–55 Ma) I- and S-type magmatism in the Gangdese arc is considered to have been generated in an accretionary tectonic setting (e.g., Zhang et al., 2010c, 2013, 2014 and references therein). The Nianbo calc-alkaline volcanic rocks of the Linzizong sequence, interpreted as the result of the Neotethyan subduction along the Yarlu–Zangpo suture, formed at ~55–50 Ma (e.g., Lee et al., 2009, 2012; Mo et al., 2008, 2009). These data synthetically suggest an eastward/northward Neotethyan subduction continuing until ~50 Ma in NW Yunnan and South Tibet.

Our amphibolitic sample (DX-62L) from Nabang in NW Yunnan shows the "white-eye socket" texture in which retrograde assemblages of plagioclase + hornblende + quartz ± biotite rim embayed garnet porphyroblasts. The metamorphic zircon of this sample gives a U–Pb age of 39.5 ± 1.4 Ma (Fig. 6a), with the crystallization core being dated at 55.3 ± 2.1 Ma (Table 2). In South Tibet and Namche Barwa, granulite- and amphibolite-facies metamorphism has been dated at 47–33 Ma (e.g., Barley et al., 2003; Cottle et al., 2009; Kohn and Parkinson, 2002; Leech et al., 2005; Najman et al. 2010; Zhang et al.,

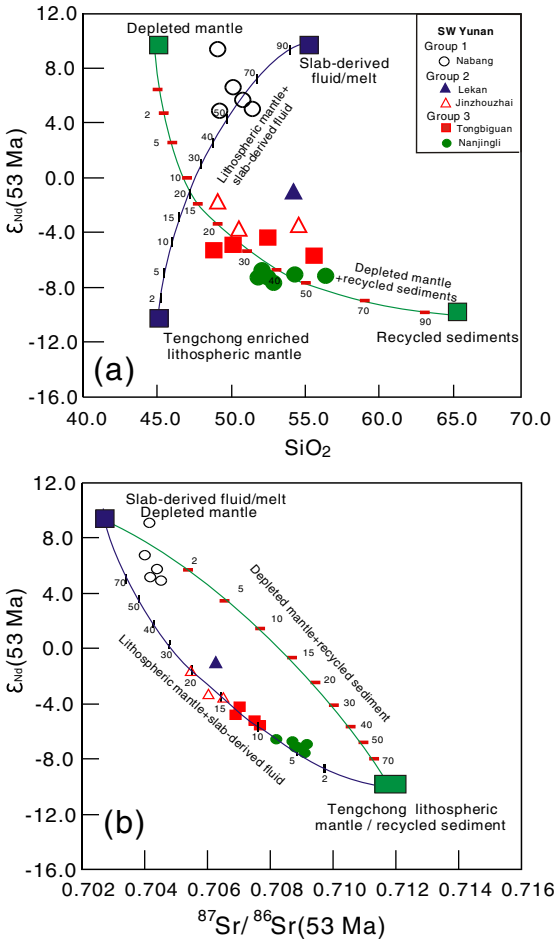

Fig. 9. Modeling calculation of (a) SiO_2 vs $\varepsilon_{Nd}(t)$ and (b) $^{87}Sr/^{86}Sr(t)$ vs $\varepsilon_{Nd}(t)$ for the metabasic rocks in SW Yunnan of the Tengchong fragment.

2010b), coinciding with a phase of magmatic quiescence (~40–26 Ma) in South Tibet and SW Yunnan (e.g., Wen et al., 2008a,b). Thus, the timing of peak metamorphism (47–33 Ma) likely corresponds with the formation of an over-thickened orogenic root beneath the Tibetan plateau. In addition, Liu et al. (2014), Smit et al. (2014) and Shellnutt et al. (2014) further considered that the crustal thickening in South Tibet was initiated at ~54–49 Ma in response to the ongoing convergence and "hard" collision of India with Eurasia (Yin, 2006). The youngest marine sedimentary rocks in South Tibet are dated at 37 Ma by Wang et al. (2003) and Najman et al. (2010). The significant deceleration of plate convergence occurred at ~52 Ma (e.g., Najman et al., 2010). The synthesis of these observations marks the transition from Neotethyan subduction to initial collision of India with Asia at ~50 Ma (e.g., Guillot et al., 2003; Leech et al., 2005; Ma et al., 2014; von Blanckenburg and Davis, 1995; Wang et al., 2014).

As introduced above, the Nabang I-type granitic rocks are the remelting products of juvenile underplated mafic rocks in an Andean-type setting (Ma et al., 2014). In the Tengchong–Gaoligong areas to east of Tongbiguan, is an extensive suite of late Cretaceous–Paleogene S-type granites. Regional relations show that the continuous northward accretion of the Burma Block probably occurred during the Jurassic to Paleocene time (e.g., Mitchell, 1993; Chung et al., 2005; Chu et al., 2006; Xu et al., 2012). This suggests a two-stage petrogenetic process for the igneous rocks involving the input of the juvenile basaltic magma and subsequent melting in the earliest Eocene in response to Neotethyan subduction. In combination with the available data, a petrogenetic model is herein proposed for the evolution of the Neotethyan Ocean during the Paleogene period and the formation of the early Eocene igneous rocks in NW Yunnan, as shown in Fig. 10a–b. During the Paleocene or earlier (>55 Ma), the Neotethyan Ocean was subducted to the north and east beneath the Eastern Burma Highlands of the Sibumasu Block, resulting in the development of the Nabang magmatic arc–back-arc system along the China–Burma border of the eastern Himalayan Syntaxis. The ongoing subduction of the Neotethyan oceanic slab facilitated the subduction of the Nabang back-arc basin beneath the Tengchong lithosphere to generate a continental arc in the Nabang–Tongbiguan area west of Nabang (Fig. 10a). Thus it is inferred that at least two northward/eastward subduction zones are involved in the suprasubduction system, resembling that proposed in South Tibet (e.g., Aitchison et al., 2002, 2007; Beck et al., 1996; Hébert et al., 2012). Subduction resulted in modification of the overlying mantle by the recycled components, which together with underplating of basaltic magma into the Tengchong crust, formed a juvenile crustal source.

In the early Eocene (55–50 Ma), the northward drift rate for the India plate decelerated from 18–19 cm/y to 4.5 cm/y (e.g., Klootwijk et al., 1992). The sudden decrease in convergence rate, along with the positive buoyancy of the Tengchong lithosphere, dampened slab subduction and stimulated its steepening to induce slab rollback (e.g., Chu et al., 2011; Ji et al., 2009, 2012; Kohn and Parkinson, 2002; Lee et al., 2009, 2012; Shellnutt et al., 2014). Such a process would mark the transition from Neotethyan subduction to initial collision of India with Asia. More importantly, such a mechanism led to thermal perturbation to facilitate partial melting of heterogeneous mantle and crustal sources, along with the accretion of voluminous deep-seated intrusions (Fig. 10b). As a result, the associated igneous rocks spatially show distinct rock-types and geochemical signatures. The melting of the MORB-like source modified by the recycled component generated Group 1 magma in the back-arc basin setting at Nabang along the China–Burma boundary. In the Nabang–Tongbiguan area, the metasomatized mantle wedge beneath the sub-arc led to the generation of the Group 2 mafic magma and juvenile crustal materials contributed to the formation of I-type granite. At the Tongbiguan–Nanjingli area, the Group 3 mafic magma and coeval S-type granites were generated at an arc but near to a within-plate environment. In summary, the petrogenesis of the early

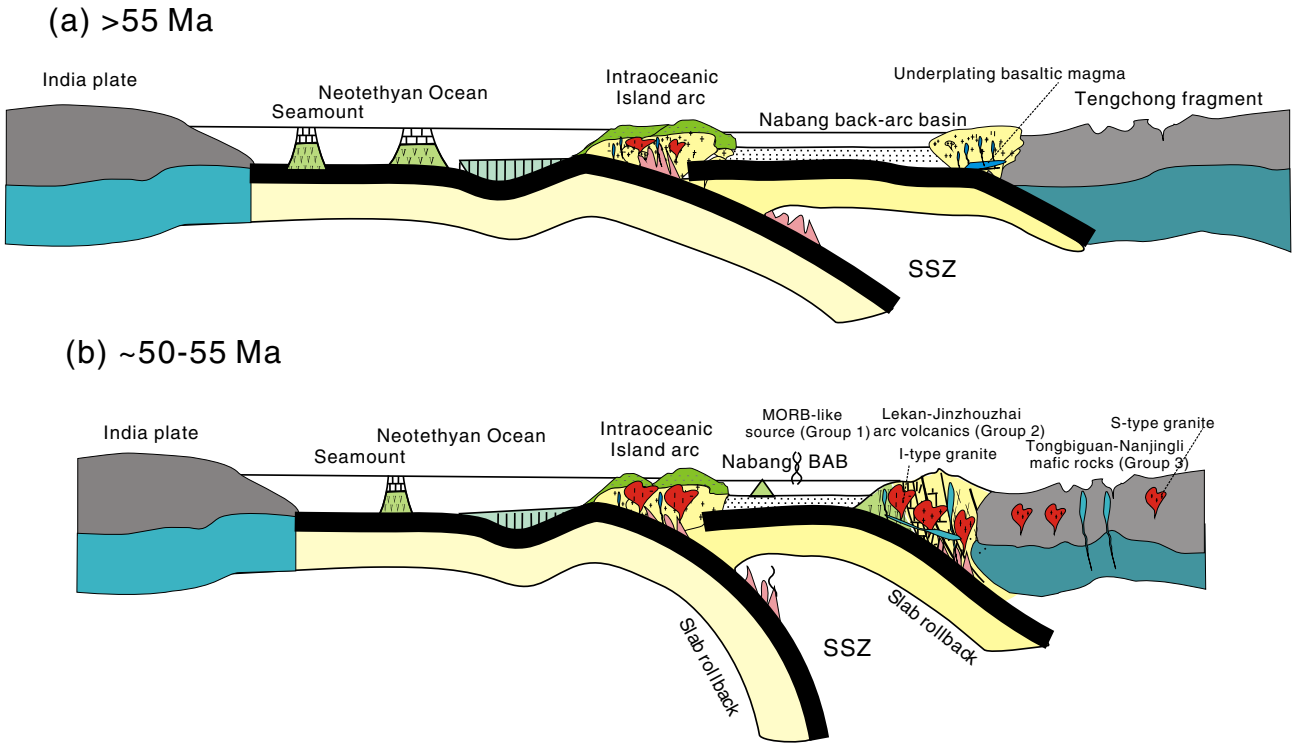

Fig. 10. Schematic cartons showing the petrogenetic model for the formation of the early Eocene igneous rocks in NW Yunnan. (a) >55 Ma, the ongoing suprasubduction of the Neotethyan slab facilitated the northward subduction of the Nabang back-arc system, resulting into the modification of the overlying lithospheric mantle and the underplating of the mafic magma into the Tengchong crust to form a juvenile crustal source. (b) 50–55 Ma, the steepening and rollback of slab in response to the sudden decrease in convergence rate and the positive buoyancy of the Tengchong lithosphere resulted in the transform from the Neotethyan subduction to initial collision of India with Asia, and induced thermal perturbation to facilitate partial melting of various sources and accretion of voluminous deep-seated intrusions in space.

Eocene (~50–55 Ma) magmatism in west Yinjiang (SW Yunnan, SW China) might be mechanically controlled by the rollback of the Neotethyan slab in the suprasubduction setting.

Supplementary data to this article can be found online at http://dx.doi.org/10.1016/j.lithos.2014.08.012.

Acknowledgments

We would like to thank X-P Xia, T-P Peng and F Guo for their help in field work. We thank the two anonymous reviewers for their thorough, critical and constructive reviews and comments, and Dr. Andrew Kerr for the helpful editorial advice. This study is financially supported by the National Basic Research Program of China (2014CB440901), "Closure of Eastern Paleotethys Ocean and Assembly of South China Continents" (41190073) of a Major NSFC Program (41190070), NSFC (41372198) and State Key Laboratory of Ore Deport Geochemistry, CAS (201301).

References

Aitchison, J.C., Davis, A.M., 2001. When did the India–Asia collision really happen? Gondwana Research 4, 560.

Aitchison, J.C., Abrajevitch, A., Ali, J.R., Badengzhu Davis, A.M., Luo, H., Liu, J.B., McDermid, I.R.C., Ziabrev, S., 2002. New insights into the evolution of the Yarlung Tsangpo suture zone, Xizang (Tibet), China. Episodes 25, 90–94.

Aitchison, J.C., Ali, J.R., Davis, A.M., 2007. When and where did India and Asia collide? Journal of Geophysical Research 112, B05423.

Barley, M., Pickard, A., Zaw, K., Rak, P., Doyle, M., 2003. Jurassic to Miocene magmatism and metamorphism in the Mogok metamorphic belt and the India–Eurasia collision in Myanmar. Tectonics 22, 1019.

Beck, R.A., Burbank, W., Sercombe, W.J., Khna, A.M., Lawrence, R.D., 1996. Late Cretaceous ophiolite obduction and Paleocene India–Asia collision in the westernmost Himalaya. Geodynamica Acta 9, 114–144.

Bédard, É., Hébert, R., Guilmette, C., Lesage, G., Wang, C.S., Dostal, J., 2009. Petrology and geochemistry of the Saga and Sangsang ophiolitic massifs, Yarlung Zangbo Suture Zone, Southern Tibet: evidence for an arc–back-arc origin. Lithos 113, 48–67.

Bezard, R., Hébert, R., Wang, C.S., Dostal, J., Dai, J.G., 2011. Petrology and geochemistry of the Xiugugabu ophiolitic massif western Yarlung Zangbo suture zone, Tibet. Lithos 125, 347–367.

Cai, F., Ding, L., Yue, Y., 2011. Provenance analysis of upper Cretaceous strata in the Tethys Himalaya, southern Tibet: implications for timing of India–Asia collision. Earth and Planetary Science Letters 305, 195–206.

Castillo, P.R., Solidum, R.U., Punogbayan, R.S., 2002. Origin of high field strength element enrichment in the Sulu Arc, southern Philippines, revisited. Geology 30, 707–710.

Castillo, P.R., Rigby, S.J., Solidum, R.U., 2007. Origin of high field strength element enrichment in volcanic arcs: geochemical evidence from the southern Sulu Arc, southern Philippines. Lithos 97, 271–288.

Chiu, H.Y., Chung, S.L., Wu, F.Y., Liu, D., Liang, Y.H., Lin, I.J., Iizuka, Y., Xie, L.W., Wang, Y., Chu, M.F., 2009. Zircon U–Pb and Hf isotopic constraints from eastern Transhimalayan batholiths on the precollisional magmatic and tectonic evolution in southern Tibet. Tectonophysics 477, 3–19.

Chu, M.F., Chung, S.L., Song, B., Liu, D., O'Reilly, S.Y., Pearson, N.J., Ji, J., Wen, D.J., 2006. Zircon U–Pb and Hf isotope constraints on the Mesozoic tectonics and crustal evolution of southern Tibet. Geology 34, 745–748.

Chu, M.F., Chung, S.L., O'Reilly, S.Y., Pearson, N.J., Wu, F.Y., Li, X.H., Liu, D., Ji, J., Chu, Q.H., Lee, H.Y., 2011. India's hidden inputs to Tibetan orogeny revealed by Hf isotopes of Transhimalayan zircons and host rocks. Earth and Planetary Science Letters 307, 479–486.

Chung, S.L., Chu, M.F., Zhang, Y., Xie, Y., Lo, C.H., Lee, T.Y., Lan, C.Y., Li, X., Zhang, Q., Wang, Y., 2005. Tibetan tectonic evolution inferred from spatial and temporal variations in post-collisional magmatism. Earth-Science Reviews 68, 173–196.

Class, C., Miller, D.M., Goldstein, S.L., Langmuir, C.H., 2000. Distinguishing melt and fluid subduction components in Umnak Volcanics, Aleutian Arc. Geochemistry, Geophysics, Geosystems 1, 1004. http://dx.doi.org/10.1029/1999GC000010.

Conticelli, S., Guarnieri, L., Farinelli, A., Mattei, M., Avanzinelli, R., Bianchini, G., Boari, E., Tommasini, S., Tiepolo, M., Prelević, D., Venturelli, G., 2009. Trace elements and Sr–Nd–Pb isotopes of K-rich, shoshonitic, and calc-alkaline magmatism of the Western Mediterranean Region: genesis of ultrapotassic to calcalkaline magmatic associations in a post-collisional geodynamic setting. Lithos 107, 68–92.

Cottle, J.M., Jessup, M.J., Newell, D.L., Horstwood, M.S.A., Noble, S.R., Parrish, R.R., Waters, D.J., Searle, M.P., 2009. Geochronology of granulitized eclogite from the Ama Drime Massif: implications for the tectonic evolution of the South Tibetan Himalaya. Tectonics 28, TC1002.

Debon, F., Le Fort, P., Sheppard, S.M.F., Sonet, J., 1986. The four plutonic belts of the Transhimalaya–Himalaya: a chemical, mineralogical, isotopic, and chronological synthesis along a Tibet–Nepal section. Journal of Petrology 27, 219–250.

Dewey, J.F., Shackleton, R.M., Chengfa, C., Yiyin, S., 1988. The tectonic evolution of the Tibetan Plateau. Philosophical Transactions of the Royal Society of London. Series A, Mathematical and Physical Sciences 327, 379–413.

Dilek, Y., Fumes, H., Shallo, M., 2008. Geochemistry of the Jurassic Mirdita Ophiolite (Albania) and the MORB to SSZ evolution of a marginal basin oceanic crust. Lithos 100, 174–209.

Ding, L., Kapp, P., Wan, X., 2005. Paleocene–Eocene record of ophiolite obduction and initial India–Asia collision, south central Tibet. Tectonics 24, TC3001.

Dong, G.C., Mo, X.X., Zhao, Z.D., Guo, T.Y., Wang, L.L., Chen, T., 2005. Geochronologic constraints on the magmatic underplating of the Gangdese belt in the India–Eurasia collision: evidence of SHRIMP II zircon U–Pb dating. Acta Geologica Sinica 79, 787–794.

Dong, G.C., Mo, X.X., Zhao, Z.D., Zhu, D.C., Wang, L.L., Chen, T., Li, B., 2006. Magma mixing in middle part of Gangdise magma belt: evidences from granitoid complex. Acta Petrologica Sinica 22, 835–844 (in Chinese with English abstract).

Dong, G.C., Mo, X.X., Zhao, Z.D., Zhu, D.C., Song, Y.T., Wang, L., 2008. Gabbros from southern Gangdese: implication for mass exchange between mantle and crust. Acta Petrologica Sinica 24, 203–210 (in Chinese with English abstract).

Elliott, T., Plank, T., Zindler, A., White, W., Bourdon, B., 1997. Element transport from slab to volcanic front at the Mariana Arc. Journal of Geophysical Research 102 (B7), 14997–15019.

Gaetani, M., Gaetani, E., 1991. Multicyclic history of the north India continental margin (northwestern Himalaya). American Association of Petroleum Geologists Bulletin 75, 1427–1446.

Gao, Y.F., Wei, R.H., Hou, Z.Q., Tian, S.H., Zhao, R.S., 2008. Eocene high-MgO volcanism in southern Tibet: new constraints for mantle source characteristics and deep processes. Lithos 105, 63–72.

Gao, Y.F., Yang, Z.S., Hou, Z.Q., Wei, R.H., Meng, X.J., Tian, S.H., 2010. Eocene potassic and ultrapotassic volcanism in south Tibet: new constraints on mantle source characteristics and geodynamic processes. Lithos 117, 20–32.

Guillot, S., Garzanti, E., Baratoux, D., Marquer, D., Mahéo, G., De Sigoyer, J., 2003. Reconstructing the total shortening history of the NW Himalaya. Geochemistry, Geophysics, Geosystems 4, 1064.

Harris, N.B.W., Ronghua, X., Lewis, C.L., Hawkesworth, C., Yuquan, Z., 1988. Isotope geochemistry of the 1985 Tibet geotraverse, Lhasa to Golmud. Philosophical Transactions of the Royal Society of London. Series A, Mathematical and Physical Sciences 263–285.

Harris, N., Inger, S., Ronghua, X., 1990. Cretaceous plutonism in Central Tibet: an example of post-collision magmatism? Journal of Volcanology and Geothermal Research 44, 21–32.

Hart, S.R., 1984. A large-scale isotope anomaly in the Southern Hemisphere mantle. Nature 309, 753–757.

Hart, S.R., 1988. Heterogeneous mantle domains: signatures, genesis and mixing chronologies. Earth and Planetary Science Letters 90, 273–296.

Hébert, R., Bezard, R., Guilmette, C., Dostal, J., Wang, C.S., Liu, Z.F., 2012. The Indus–Yarlung Zangbo ophiolites from Nanga Parbat to Namche Barwa syntaxes, southern Tibet: first synthesis of petrology, geochemistry, and geochronology with incidences on geodynamic reconstructions of Neo-Tethys. Gondwana Research 22, 377–397.

Hickey-Vargas, R., 1998. Origin of the Indian ocean-type isotopic signature in basalts from Philippine Sea plate spreading centers: an assessment of local versus large-scale processes. Journal of Geophysical Research 103, 20,963–20,979.

Hodges, K.V., 2000. Tectonics of the Himalaya and southern Tibet from two perspectives. Geological Society of America Bulletin 112, 324–350.

Hofmann, A.W., 1997. Mantle geochemistry: the message from oceanic volcanism. Nature 385, 219–229.

Hu, X., Sinclair, H.D., Wang, J., Jiang, H., Wu, F., 2012. Late Cretaceous–Palaeogene stratigraphic and basin evolution in the Zhepure Mountain of southern Tibet: implications for the timing of India–Asia initial collision. Basin Research 24, 520–543.

Huang, Y., Zhao, Z.D., Zhang, F.Q., Zhu, D.C., Dong, G.C., Mo, X.X., 2010. Geochemistry and implication of the Gangdese batholiths from Renbu and Lhasa areas in southern Gangese, Tibet. Acta Petrologica Sinica 26, 3131–3142 (in Chinese with English abstract).

Jaeger, J.J., Courtillot, V., Tapponnier, P., 1989. Paleontological view of the ages of the Deccan Traps, the Cretaceous/Tertiary boundary, and the India–Asia collision. Geology 17, 316–319.

Ji, J.Q., Zhong, D.L., Shang, H.Q., Qiu, J., Hu, S.L., 2000a. Dating of two metamorphic events on the basalt granulite from the Nabang area on the border of China and Burma. Acta Petrologica Sinica 16, 227 (in Chinese with English abstract).

Ji, J.Q., Zhong, D.L., Chen, C.Y., 2000b. Geochemistry and genesis of Nabang metamorphic basalt, southwest Yunnan, China: implications for the subducted slab break-off. Acta Petrologica Sinica 16, 433–442 (in Chinese with English abstract).

Ji, W.Q., Wu, F.Y., Chung, S.L., Li, J.X., Liu, C.Z., 2009. Zircon U–Pb geochronology and Hf isotopic constraints on petrogenesis of the Gangdese batholith, southern Tibet. Chemical Geology 262, 229–245.

Ji, W.Q., Wu, F.Y., Liu, C.Z., Chung, S.L., 2012. Early Eocene crustal thickening in southern Tibet: new age and geochemical constraints from the Gangdese batholith. Journal of Asian Earth Sciences 53, 82–95.

Kapp, J.L.D.A., Harrison, T.M., Kapp, P., Grove, M., Lovera, O.M., Lin, D., 2005. Nyainqentanglha Shan: a window into the tectonic, thermal, and geochemical evolution of the Lhasa block, southern Tibet. Journal of Geophysical Research 110, B08413.

Klootwijk, C.T., Gee, J.S., Peirce, J.W., Smith, G.M., McFadden, P.L., 1992. An early India–Asia contact: paleomagnetic constraints from Ninetyeast Ridge, ODP Leg 121. Geology 20, 395–398.

Köhler, J., Schönenberger, J., Upton, B., Markl, G., 2009. Halogen and trace-element chemistry in the Gardar Province, South Greenland: subduction-related mantle metasomatism and fluid resolution from alkalic melts. Lithos 113, 731–747.

Kohn, M.J., Parkinson, C.D., 2002. Petrologic case for Eocene slab breakoff during the Indo-Asian collision. Geology 30, 591–594.

Lee, H.Y., Chung, S.L., Lo, C.H., Ji, J., Lee, T.Y., Qian, Q., Zhang, Q., 2009. Eocene Neotethyan slab breakoff in southern Tibet inferred from the Linzizong volcanic record. Tectonophysics 477, 20–35.
Lee, H.Y., Chung, S.L., Ji, J., Qian, Q., Gallet, S., Lo, C.H., Lee, T.Y., Zhang, Q., 2012. Geochemical and Sr–Nd isotopic constraints on the genesis of the Cenozoic Linzizong volcanic successions, southern Tibet. Journal of Asian Earth Sciences 53, 96–114.
Leech, M.L., Singh, S., Jain, A.K., Klemperer, S.L., Manickavasagam, R.M., 2005. The onset of India–Asia continental collision: early, steep subduction required by the timing of UHP metamorphism in the western Himalaya. Earth and Planetary Science Letters 234, 83–97.
Li, X.H., Li, W.X., Wang, X.C., Li, Q.L., Liu, Y., Tang, G.Q., Gao, Y.Y., Wu, F.Y., 2010a. SIMS U–Pb zircon geochronology of porphyry Cu–Au–(Mo) deposits in the Yangtze River Metallogenic Belt, eastern China: magmatic response to early Cretaceous lithospheric extension. Lithos 119, 427–438.
Li, X.H., Li, W.X., Wang, X.C., Li, Q.L., Liu, Y., Tang, G.Q., Gao, Y.Y., Wu, F.Y., 2010b. SIMS U–Pb zircon geochronology of porphyry Cu–Au–(Mo) deposits in the Yangtze River Metallogenic Belt, eastern China: magmatic response to early Cretaceous lithospheric extension. Lithos 119, 427–438.
Liang, X.R., Wei, G.J., Li, X.H., Liu, Y., 2003. Precise measurement of $^{143}Nd/^{144}Nd$ and Sm/Nd ratios using multiple-collectors inductively coupled plasma-mass spectrometer (MC-ICPMS). Geochimica 32, 91–96.
Liu, D., Zhao, Z.D., Zhu, D.C., Niu, Y.L., Harrison, T.M., 2014. Zircon xenocrysts in Tibetan ultrapotassic magmas: imaging the deep crust through time. Geology 42, 43–46.
Luhr, J.F., Haldar, D., 2006. Barren Island Volcano (NE Indian Ocean): island-arc high-alumina basalts produced by troctolite contamination. Journal of Volcanology and Geothermal Research 149, 177–212.
Ma, L.Y., Wang, Y.J., Fan, W.M., Geng, H.Y., Cai, Y.F., Zhong, F., Liu, H.C., Xing, X.W., 2014. Petrogenesis of the early Eocene I-type granites in west Yingjiang (SW Yunnan) and its implication for the eastern extension of the Gangdese batholiths. Gondwana Research 25, 401–419.
Meschede, M., 1986. A method of discriminating between different types of mid-ocean ridge basalts and continental tholeiites with the Nb–Zr–Y diagram. Chemical Geology 56, 207–218.
Metcalfe, I., 1996. Gondwanaland dispersion, Asian accretion and evolution of eastern Tethys. Australian Journal of Earth Sciences 43, 605–623.
Metcalfe, I., 1998. Palaeozoic and Mesozoic geological evolution of the SE Asian region: multidisciplinary constraints and implications for biogeography. Biogeography and Geological Evolution of SE Asia 25–41.
Middlemost, E.A.K., 1994. Naming materials in the magma/igneous rock system. Earth-Science Reviews 37, 215–224.
Mitchell, A.H.G., 1993. Cretaceous–Cenozoic tectonic events in the western Myanmar (Burma)–Assam region. Journal of the Geological Society 150, 1089–1102.
Mo, X.X., Zhao, Z.D., Zhou, S., Dong, G.C., Guo, T., Wang, L., 2002. Evidence for timing of the initiation of India–Asia collision from igneous rocks in Tibet. AGU Fall Meeting Abstracts 1201.
Mo, X.X., Dong, G.C., Zhao, Z.D., Zhou, S., Wang, L.L., Qiu, R.Z., Zhang, F.Q., 2005. Spatial and temporal distribution and characteristics of granitoids in the Gangdese, Tibet and implication for crustal growth and evolution. Geological Journal of China Universities 11, 281–290.
Mo, X.X., Hou, Z.Q., Niu, Y.L., Dong, G.C., Qu, X.M., Zhao, Z.D., Yang, Z.M., 2007. Mantle contributions to crustal thickening during continental collision: evidence from Cenozoic igneous rocks in southern Tibet. Lithos 96, 225–242.
Mo, X.X., Niu, Y.L., Dong, G.C., Zhao, Z.D., Hou, Z.Q., Zhou, S., Ke, S., 2008. Contribution of syncollisional felsic magmatism to continental crust growth: a case study of the Paleogene Linzizong volcanic succession in southern Tibet. Chemical Geology 250, 49–67.
Mo, X.X., Dong, G.C., Zhao, Z.D., Zhu, D.C., Zhou, S., Niu, Y.L., 2009. Mantle input to the crust in southern Gangdese, Tibet, during the Cenozoic: zircon Hf isotopic evidence. Journal of Earth Science 20, 241–249.
Morley, C., Woganan, N., Sankumarn, N., Hoon, T., Alief, A., Simmons, M., 2001. Late Oligocene–Recent stress evolution in rift basins of northern and central Thailand: implications for escape tectonics. Tectonophysics 334, 115–150.
Najman, Y., Appel, E., Boudagher-Fadel, M., Bown, P., Carter, A., Garzanti, E., Godin, L., Han, J., Liebke, U., Oliver, G., 2010. Timing of India–Asia collision: geological, biostratigraphic, and palaeomagnetic constraints. Journal of Geophysical Research 115, B12416.
Nelson, D.R., 1992. Isotopic characteristics of potassic rocks: evidence for the involvement of subducted sediments in magma genesis. Lithos 28, 403–420.
Owens, T.J., Zandt, G., 1997. Implications of crustal property variations for models of Tibetan plateau evolution. Nature 387, 37–43.
Pan, G.T., Wang, L.Q., Li, R.S., Yuan, S.H., Ji, W.H., Yin, F.G., Zhang, W.P., Wang, B.D., 2012. Tectonic evolution of the Qinghai–Tibet Plateau. Journal of Asian Earth Sciences 53, 2–14.
Pearce, J.A., Cann, J.R., 1973. Tectonic setting of basic volcanic rocks determined using trace element analyses. Earth and Planetary Science Letters 19, 290–300.
Pearce, J.M., Peate, D.W., 1995. Tectonic implications of the composition of volcanic arc magmatism. Annual Review of Earth and Planetary Sciences 23, 251–285.
Pearce, J.A., Harris, N.B.W., Tindle, A.G., 1984. Trace element discrimination diagrams for the tectonic interpretation of granitic rocks. Journal of Petrology 25, 956–983.
Pearce, J.A., Baker, P.E., Harvey, P.K., Luff, I.W., 1995. Geochemical evidence for subduction fluxes, mantle melting and fractional crystallization beneath the South Sandwich island arc. Journal of Petrology 36, 1073–1109.
Peng, T.P., Wang, Y.J., Fan, W.M., Liu, D.Y., Shi, Y.R., Miao, L.C., 2006. SHRIMP zircon U–Pb geochronology of early Mesozoic felsic igneous rocks from the southern Lancangjiang and its tectonic implications. Science in China Series D: Earth Sciences 49, 1032–1042.
Petrone, C.M., Ferrari, L., 2008. Quaternary adakite-Nb-enriched basalt association in the western Trans-Mexican Volcanic Belt: is there any slab melt evidence? Contributions to Mineralogy and Petrology 156, 73–86.
Plank, T., 2005. Constraints from thorium/lanthanum on sediment recycling at subduction zones and the evolution of the continents. Journal of Petrology 46, 921–944.
Reagan, M.K., Ishizuka, O., Stern, R.J., Kelley, K.A., Blichert-Toft, J., Bloomer, S.H., Cash, J., Fryer, P., Hanan, B.B., Hickey-Vargas, R., Ishii, T., Kimura, J., Peate, D.W., Rowe, M.C., Woods, M., 2010. Fore-arc basalts and subduction initiation in the Izu–Bonin–Mariana system. Geochemistry, Geophysics, Geosystems 11, Q03X12. http://dx.doi.org/10.1029/2009GC002871.
Replumaz, A., Tapponnier, P., 2003. Reconstruction of the deformed collision zone between India and Asia by backward motion of lithospheric blocks. Journal of Geophysical Research 108, 2285.
Rolland, Y., Mahéo, G., Pêcher, A., Villa, I.M., 2009. Syn-kinematic emplacement of the Pangong metamorphic and magmatic complex along the Karakorum Fault (N Ladakh). Journal of Asian Earth Sciences 34 (1), 10–25.
Rowley, D.B., 1996. Age of initiation of collision between India and Asia: a review of stratigraphic data. Earth and Planetary Science Letters 145, 1–13.
Sandeman, H.A., Hanmer, S., Tella, S., Armitage, A.A., Davis, W.J., Ryand, J.J., 2006. Petrogenesis of Neoarchaean volcanic rocks of the MacQuoid supracrustal belt: a back-arc setting for the northwestern Hearne subdomain, western Churchill Province, Canada. Precambrian Research 144 (1–2), 126–139.
Searle, M.P., Windley, B.F., Coward, M.P., Cooper, D.J.W., Rex, A.J., Rex, D.C., Tingdong, L., Xuchang, X., Jan, M.Q., Thakur, V.C., 1987. The closing of Tethys and the tectonics of the Himalaya. Geological Society of America Bulletin 98, 678–701.
Shellnutt, J.G., Lee, T.Y., Brookfield, M.E., Chung, S.L., 2014. Correlation between magmatism of the Ladakh Batholith and plate convergence rates during the India–Eurasia collision. Gondwana Research http://dx.doi.org/10.1016/j.gr.2013. 09.006.
Shinjo, R., Chung, S.L., Kato, Y., Kimura, M., 1999. Geochemical and Sr–Nd isotopic characteristics of volcanic rocks from the Okinawa Trough and Ryukyu arc: implications for the evolution of a young, intracontinental back arc basin. Journal of Geophysical Research 104 (5), 10591–10608.
Smit, M.A., Hacker, B.R., Lee, J., 2014. Tibetan Garnet Records Early Eocene Initiation of Thickening in the Himalaya. http://dx.doi.org/10.1130/G35524.1.
Song, S., Niu, Y., Wei, C., Ji, J., Su, L., 2010. Metamorphism, anatexis, zircon ages and tectonic evolution of the Gongshan block in the northern Indochina continent—an eastern extension of the Lhasa Block. Lithos 120, 327–346.
Sun, S.S., McDonough, W.F., 1989. Chemical and isotopic systematics of oceanic basalts: implications for mantle composition and processes. In: Saunders, A.D., Norry, M.J. (Eds.), Magmatism in the Ocean Basins. Geological Society of Special Publication. 42, pp. 313–345.
Tommasini, S., Avanzinelli, R., Conticelli, S., 2011. The Th/La and Sm/La conundrum of the Tethyan realm lamproites. Earth and Planetary Science Letters 301, 469–478.
Ueno, K., 2000. Permian fusulinacean faunas of the Sibumasu and Baoshan Blocks: implications for the paleogeographic reconstruction of the Cimmerian continent. Geosciences Journal 4, 160–163.
von Blanckenburg, F., Davis, J.H., 1995. Slab breakoff: a model for syncollisional magmatism and tectonics in the Alps. Tectonics 14, 120–131.
Wang, Y., 1983. The characteristics and significance of Carboniferous gravel beds in the Tengchong and Baoshan area, western Yunnan. In: Zhou, Z., Xu, X., Zhou, W. (Eds.), Geology of Qinghai–Xizang (Tibet) Plateau. Beijing. 11, pp. 71–77 (in Chinese with English abstract).
Wang, C.S., Li, X.H., Hu, X.M., 2003. Age of initial collision of India with Asia: review and constraints from sediment s in southern Tibet. Acta Geologica Sinica 77, 16–24 (in Chinese with English abstract).
Wang, Y.J., Fan, W.M., Zhang, Y.H., Peng, T., Chen, X.Y., Xu, Y.G., 2006. Kinematics and $^{40}Ar/^{39}Ar$ geochronology of the Gaoligong and Chongshan shear systems, western Yunnan, China: implications for early Oligocene tectonic extrusion of SE Asia. Tectonophysics 418, 235–254.
Wang, Y.J., Zhang, A.M., Fan, W.M., Zhang, Y.H., 2013. Origin of paleosubduction-modified mantle for Silurian gabbro in the Cathaysia Block: geochronological and geochemical evidence. Lithos 160, 37–54.
Wang, Y.J., Li, S.B., Ma, L.Y., Fan, W.M., Cai, Y.F., Zhang, Y.H., Zhang, F.F., 2014. Geochronological and geochemical constraints on the petrogenesis of Early Eocene metagabbroic rocks in Nabang (SW Yunnan) and its implications on the Neotethyan slab subduction. Gondwana Research http://dx.doi.org/10.1016/j.gr.2014.01.007.
Wei, G.J., Liang, X.R., Li, X.H., Liu, Y., 2002. Precise measurement of Sr isotopic composition of liquid and solid base using (LP) MC–ICPMS. Geochimica 31, 295–299.
Wen, D.R., Chung, S.L., Song, B., Iizuka, Y., Yang, H.J., Ji, J., Liu, D., Gallet, S., 2008a. Late Cretaceous Gangdese intrusions of adakitic geochemical characteristics, SE Tibet: petrogenesis and tectonic implications. Lithos 105, 1–11.
Wen, D.R., Liu, D., Chung, S.L., Chu, M.F., Ji, J., Zhang, Q., Song, B., Lee, T.Y., Yeh, M.W., Lo, C. H., 2008b. Zircon SHRIMP U–Pb ages of the Gangdese Batholith and implications for Neotethyan subduction in southern Tibet. Chemical Geology 252, 191–201.
Wood, D.A., 1980. The application of a Th–Hf–Ta diagram to problems of tectonomagmatic classification and to establishing the nature of crustal contamination of basaltic lavas of the British Tertiary Volcanic Province. Earth and Planetary Science Letters 50, 11–30.
Wu, H., Boulter, C., Ke, B., Stow, D., Wang, Z., 1995. The Changning–Menglian suture zone; a segment of the major Cathaysian–Gondwana divide in Southeast Asia. Tectonophysics 242, 267–280.
Xia, X., Sun, M., Geng, H.Y., Sun, Y., Wang, Y., Zhao, G., 2011. Quasi-simultaneous determination of U–Pb and Hf isotope compositions of zircon by excimer laser-ablation multiple-collector ICPMS. Journal of Analytical Atomic Spectrometry 26, 1868–1871.

Xie, K.J., Zeng, L.S., Liu, J., Gao, L.E., HU, G.Y., 2011. Timing and geochemistry of the Linzizong Group volcanic rocks in Sangsang area, Ngamring County, southern Tibet. Geological Bulletin of China 30, 1139–1352 (in Chinese with English abstract).

Xu, Y.G., Yang, Q.J., Lan, J.B., Luo, Z.Y., Huang, X.L., Shi, Y.R., Xie, L.W., 2012. Temporal–spatial distribution and tectonic implications of the batholiths in the Gaoligong–Tengliang–Yingjiang area, western Yunnan: constraints from zircon U–Pb ages and Hf isotopes. Journal of Asian Earth Sciences 53, 151–175.

Yang, C., Xia, G., Deng, R., 2002. Characteristics of dulongjiang granite and magmatism in northwest Yunnan. Yunnan Geology 1, 21–33 (in Chinese with English abstract).

Yin, A., 2006. Cenozoic tectonic evolution of the Himalayan orogen as constrained by along-strike variation of structural geometry, exhumation history, and foreland sedimentation. Earth Science Reviews 76, 1–131.

Yin, A., Harrison, T.M., 2000. Geologic evolution of the Himalayan–Tibetan orogen. Annual Review of Earth and Planetary Sciences 28, 211–280.

Yue, Y.H., Ding, L., 2006. $^{40}Ar/^{39}Ar$ geochronology, geochemical characteristics and genesis of the Linzhou basic dikes, Tibet. Acta Petrologica Sinica 22, 855–866 (in Chinese with English abstract).

Yunnan BGMR (Yunnan Bureau of Geology and Mineral Resources), 1990. Regional Geology of the Yunnan Province. Geological Publishing House, Beijing, p. 592, (in Chinese with English abstract).

Zhang, B., Zhang, J., Zhong, D., 2010a. Structure, kinematics and ages of transpression during strain-partitioning in the Chongshan shear zone, western Yunnan, China. Journal of Structural Geology 32, 445–463.

Zhang, Z.M., Zhao, G.C., Santosh, M., Wang, J.L., Dong, X., Liou, J.G., 2010b. Two-stages of granulite-facies metamorphism in the eastern Himalayan Syntaxis, south Tibet: petrology, zircon geochronology and implications for the subduction of Neo-Tethys and the Indian continent beneath Asia. Journal of Metamorphic Geology 28, 719–733.

Zhang, Z.M., Zhao, G.C., Santosh, M., Wang, J.L., Dong, X., Shen, K., 2010c. Late Cretaceous charnockite with adakitic affinities from the Gangdese batholith, southeastern Tibet: evidence for Neo-Tethyan mid-ocean ridge subduction? Gondwana Research 17, 615–631.

Zhang, Z.M., Dong, X., Xiang, H., Liou, J.G., Santosh, M., 2013. Building of the deep Gangdese arc, South Tibet Paleocene plutonism and granulite-facies metamorphism. Journal of Petrology 54, 2508–2547.

Zhang, Z.M., Dong, X., Santosh, M., Zhao, G.C., 2014. Metamorphism and tectonic evolution of the Lhasa terrane, Central Tibet. Gondwana Research 25, 170–189.

Zhao, Z.D., Zhu, D.C., Dong, G.C., Mo, X.X., DePaolo, D., Jia, L.L., Hu, Z.C., Yuan, H.L., 2011. The ~54 Ma gabbro–granite intrusive in southern Dangxung area, Tibet: petrogenesis and implications. Acta Petrologica Sinica 27, 3513–3524.

Zhong, D., 1998. Paleo-Tethyan Orogenic Belt in the Western Parts of the Sichuan and Yunnan Provinces. Science Press, Beijing, pp. 1–231, (in Chinese with English abstract).

Zhu, D.C., Mo, X.X., Niu, Y., Zhao, Z.D., Wang, L.Q., Pan, G.T., Wu, F.Y., 2009. Zircon U–Pb dating and in-situ Hf isotopic analysis of Permian peraluminous granite in the Lhasa terrane, southern Tibet: implications for Permian collisional orogeny and paleogeography. Tectonophysics 469, 48–60.

Zhu, D.C., Zhao, Z.D., Niu, Y., Mo, X.X., Chung, S.L., Hou, Z.Q., Wang, L.Q., Wu, F.Y., 2011. The Lhasa Terrane: record of a microcontinent and its histories of drift and growth. Earth and Planetary Science Letters 301, 241–255.

Zhu, D.C., Zhao, Z.D., Niu, Y.L., Dilek, Y., Hou, Z.Q., Mo, X.X., 2012. The origin and pre-Cenozoic evolution of the Tibetan Plateau. Gondwana Research 23, 1429–1454.